MINERALOGY, ALTERATION

AND

GEOCHEMICAL STUDIES

OF THE

SAN LUIS GOLD DEPOSIT
COSTILLA COUNTY, COLORADO

by

Abdelaziz Kaina

Submitted in Partial Fulfillment
of the Requirements for the Degree of
Master of Science in Geochemistry

New Mexico Institute of Mining and Technology
Socorro, New Mexico
August 1993

ACKNOWLEDGMENTS

I am indebted to my academic advisor Dr. David Norman, for suggesting this project and for many helpful, stimulating discussions and guidance ; to Dr. Andrew Campbell and Dr. R. W. Ohline.

I would like to thank Francis Agezo. His professional advice, enthusiasm and help in the field and discussion have been invaluable to me. And also Randy for the help and time he provided me with the computer work.

This project was supported by the United States Agency for the International Development.

ABSTRACT

The San Luis gold deposit, located in the western foothills of the Sangre de Cristo mountains in San Luis basin, south central Colorado, contains 11,021,000 tonnes of ore at 1.4 g/t gold in two mineable zones. The tabular ore bodies are hosted by the Precambrian biotite gneiss breccia, along a low-angle detachment fault zone. The San Luis basin is interpreted to be an integral part of the Rio Grande rift system, formed during Neogene and Quaternary time which corresponds to the late volcanic activities that lasted from Miocene to Pliocene time in San Juan mountains and in the San Luis valley.

Detailed Studies of the mine area have shown that the gold associated hydrothermal alteration is characterised by relative enrichment in K_2O, SiO_2 and Fe_2O_3, and depletion in Na_2O, CaO and MgO, which produced systematic trends of alteration mineral assemblages. The hydrothermal alteration sequence, consists of sericitc alteration, succeded in space by a weak argillic alteration and finally propylitic alteration which is associated with less intense altered rocks. The variations of K_2O, SiO_2, Fe_2O_3, Na_2O, CaO and MgO abundance in mine area reveal a remarkable correspondence to variations of gold abundance, suggesting a genetic relationship of gold enrichment to hydrothermal alteration. The gold mineralization is associated with silicification and quartz-sericite-pyrite alteration. Ore mineralogy , alteration types, metallic elements present and the structural control of the low-angle fault zone mineralization have allowed to classify San Luis deposit as a detachment related epithermal deposit.

Geochemical data has shown that the depositing fluid was polymetallic event and has also revealed that gold is a part of the quartz-sericite-pyrite mineral assembly.

Fluid inclusion studies indicate mineralization by low salinity fluid down to 0 eq.wt% Na Cl over temperature ranges of 230 to 280 ^{o}c. The calculated variations in enthalpy of the hydrothermal fluid suggest that a fluid cooling mechanism responsible was responsible for ore deposition. Hot, relatively pure water, metal-rich fluid ascended, intersected the low-angle fault zone and cooled to cause precipitation of iron, copper, lead, zinc and gold.

TABLE OF CONTENTS

INTRODUCTION

STATEMENT OF PROBLEMS

The previous studies on San Luis deposit were mostly descriptive and neither detailed alteration nor fluid inclusion and geochemical studies have been carried out. San Luis is a unique type of ore deposit occurring on low angle structure in Precambrian rocks. This study was undertaken with the following objectives in mind, to characterize the mineralogy of the deposit, to determine the zonation of minerals in the district and to document the alteration associated with the mineralization. These are aimed at determining the geochemical environment of ore deposition and at classifying the deposit.

LOCATION AND DESCRIPTION

The San Luis deposits are located about 5 miles northeast of the town of San Luis in Costilla County, south-central Colorado (fig. 1). The Sangre de Cristo Mountains are a northerly trending chain of 3,657 to 4,267 m peaks which extend over 340 km from Santa Fe, New Mexico to Salida, Colorado (Benson, 1990). The San Luis deposit lies in the western slope of the range at the east edge of the San Luis basin (Jones and Benson, 1990). The deposit topography consists of gentle southern dipping slopes at the altitude from 2400

m to over 2700 m. The gold deposit is located in the vicinity of a major structure, termed the clay fault zone. The ore bodies which occur in a biotite gneiss, have been exposed over an area of about 1000 by 1600 m (Gunther, 1905).The mine receives an average rainfall of 12" annually. The Rito Seco flows westward, across the southern part of the mine property. Sagebrush, juniper and pinon pine are the dominant vegetation in the area.

Figure 1. Location map of the San Luis deposit and the San Luis Basin (modified from Keller, et al, 1984)

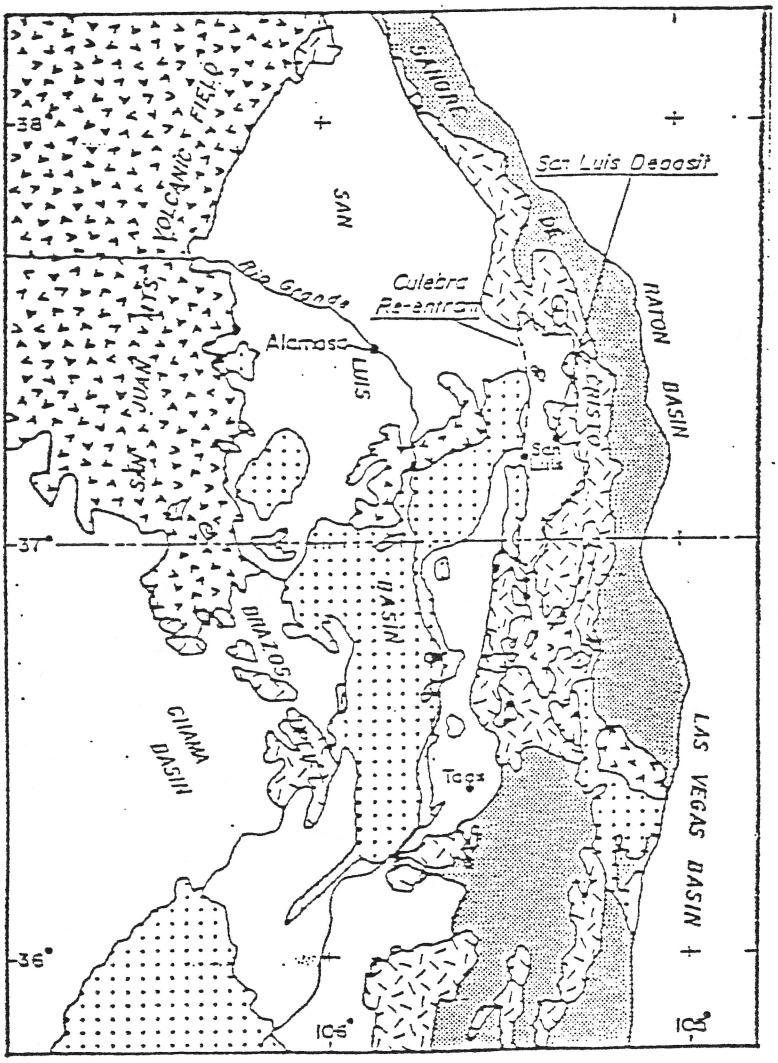
38°
37°
36°
105°
SAN JUAN MTS.
VOLCANIC FIELD of
SAN LUIS BASIN
GUADALOUPE
San Luis Deposit
Culebra Re-entrant
Rio Grande
Alamosa
RATON BASIN
CHAMA BASIN
Taos
LAS VEGAS BASIN
EXPLANATION
Sedimentary rocks Miocene to Holocene
Miocene and younger igneous rocks
Cretaceous and older sedimentary rocks
Oligocene and older igneous rocks
Precambrian rocks
0 5 10 20 30 miles
0 5 10 20 30 40 50 kilometers

PREVIOUS WORK

The Geology of the San Luis area has been described by Gunther (1905); Benson and Jones (1990) and most recently again by Benson and Jones (unpublished paper 1991). The latter's work is extensively quoted in the following brief outline of the regional and local geology.

REGIONAL SETTING

Basement lithologies in the Sangre de Cristo Mountains consists of 1800 Ma proterozoic gneisses which have been intruded by 1,700 and 1,400 Ma granites (Tweto, 1979) (fig. 2). Poorly sorted, high-energy sediments of the Miocene to Pliocene Santa Fe Group partially overlie the deposit and mark the eastern edge of the Neogene San Luis depositional basin. The eastern half of the range consists dominantly of Paleozoic sedimentary rocks which are steeply overturned and folded during Laramide orogenic events. Synchronous with the recent relative uplift of the range, which is inferred to have occurred during Neogene and Quaternary time, was the development of the San Luis basin and deposition of the sediment formations. San Luis basin is an integral part of the Rio Grande rift system. Chapin et al., 1992, concluded also that San Luis basin was formed as a broad half graben tilted to the east; It was filled with sediments of the latest Oligocene to Pleistocene Santa Fe group derived from

the rising Sangre de Cristo and San Juan mountains. The range of Sangre de Cristo is bordered by the deepest sides of the half grabens of San Luis basin on the west and with mountain valley on the east. Chapin et al., 1992, concluded that a mountain blocks with young FT (fission track) ages reflect an isostatic response to large scale displacements along the major half graben bounding faults. Chapin et al., 1992 summarized that near surface features such as asymmetric and rotated structures, large local relief, and the amount of denudation predicted from FT data, are more readily explained in terms of localized isostatic flexures. It appears that the San Luis deposit lies within a failed part of the Rio Grande rift where tertiary sedimentary rocks are preserved at a higher structural level (Benson et al., 1990). Small Tertiary dikes of rhyolite and andesite of less than 10 m thick are present at the mine area. The nearest volumetrically significant Tertiary intrusions are the 26-24 Ma Questa magmatic system to the south (Lipman et al., 1986), the 25-19 Ma Spanish Peaks system to the east (Tweto, 1979), and small sill-like intrusions near La Veta pass to the north.

The volcanic history of the San Juan mountains has been described by Steven et al., 1970, and Steven and Lipman 1976, and Lipman et al., 1978. Volcanic activities probably began in latest Eocene or early Oligocene time with the eruption of andesitic lavas from many widespread centers. The volcanism was especially intense between 30 and 35 Ma and formed major large volcanic field that covered most of the southern Rocky mountains, (Steven et al., 1968;

Steven 1975). Following the andesitic lavas, approximately 30 Ma, eruptions of quartz latitic and rhyolitic ash flows started (Lipman et al., 1978).

Approximately 25 Ma the character of volcanism changed from quartz latite and low silica rhyolite to bimodal suite of basaltic lavas and high silica, alkali rich rhyolite (Lipman et al., 1970). This early Miocene volcanic activity was accompanied by the onset of basin and range faulting to the east of the San Juan mountains in the San Luis valley segment of the Rio Grande (Lipman and Mehnert, 1975). The scarp bordering the graben of San Luis valley is mainly in Precambrian rocks although sedimentary rocks cap the crest of the range in many places. Basalt and rhyolite eruptions accompanied by rifting continued intermittently into Pliocene time (Tweto, 1970).

Figure 2. Generalized Geology of the San Luis Deposit

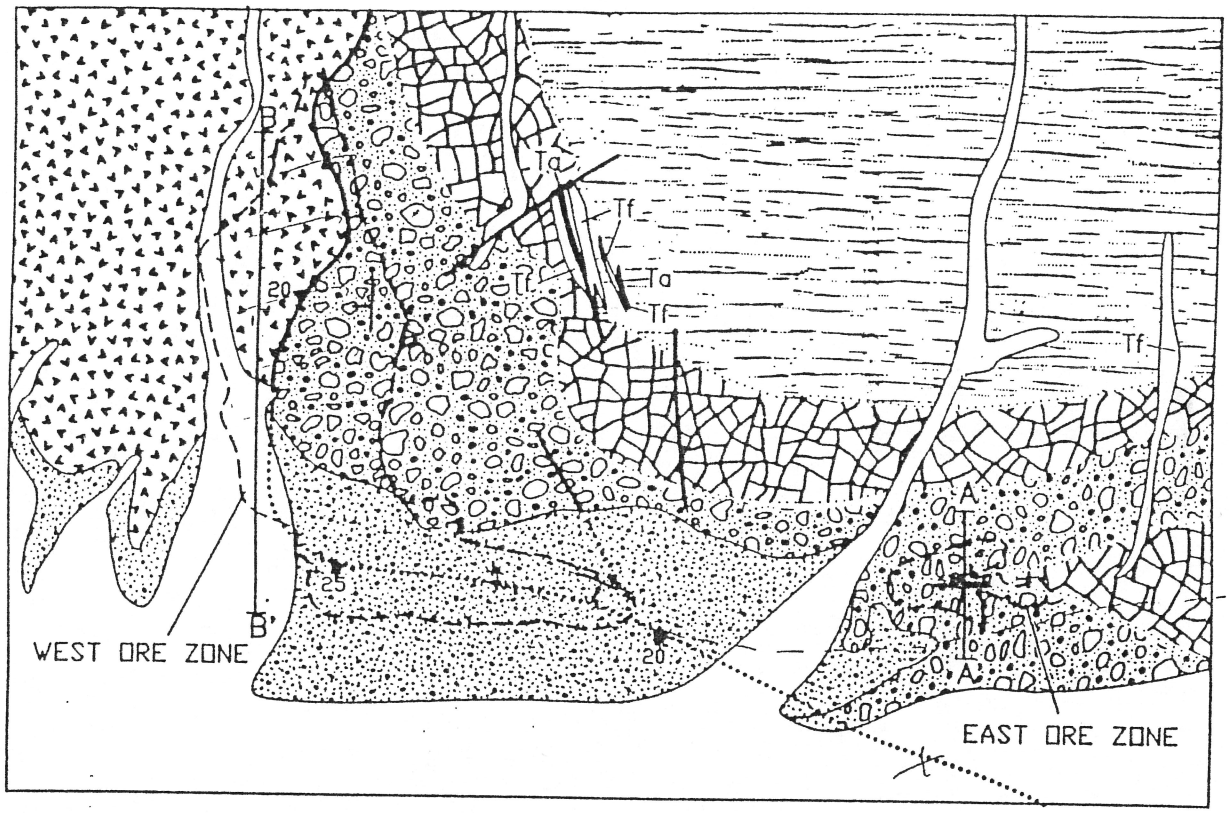

0 1000 FEET 2000 3000

0 1 2 3 4

KILOMETERS

LOCATION OF MAP AREA

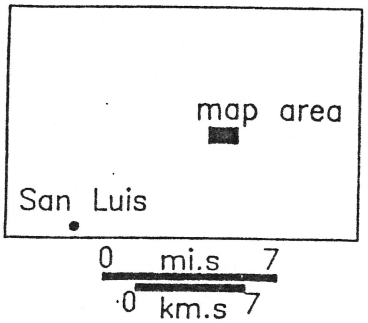

Tertiary
- alluvium
- Santa Fe Formation
- Ta andesite
- Tf felsite

Precambrian
- biotite gneiss breccia
- biotite gneiss cataclasite
- gneissic granite
- biotite gneiss

- faults (dotted where inferred)
- surface projection of ore contours (>0.0169 oz/st Au)
- detachment fault, teeth on hanging wall (dotted where inferred)

HISTORY OF MINING

Mineralization at San Luis was first reported probably late 16th or early 17th Century when Spanish expeditions from Mexico went searching for the Golden Cities of Cibola. Production began 1890. The principal metals mined were lead and silver. The historical name for the San Luis deposit was "EL Plomo" because of the presence of galena. From 1897 through 1934 gold was produced intermittently (Benson and Jones, 1990).

San Luis was leased by ASARCO in 1931 and 1959, and by Inspiration Copper Co. in 1968. In 1972 Earth Science, Inc. (ESI) leased and delineated parts of the east and west ore zones. Battle Mountain Gold Company (BMGC) optioned San Luis in May 1987. Development and feasibility work continued through 1988 after initial drilling in August 1987. Reconnaissance prospecting surveys were carried out at San Luis, and the permit to mine was issued by the state of Colorado Mined Land Reclamation Division in March, 1988.

The estimated reserves are 11,021,500 tonnes of ore at 1.4 g/t of gold in two zones: The east ore zone which lies in the extreme east portion of the mine, contains 1,277,300 tonnes at an average grade of 1.68 g/t. The west ore zone in the Central and western portion of the mine property contains 9,744,000 tonnes with an average grade of 1.34 g/t of gold (fig. 2; Johnson, 1989).

LOCAL GEOLOGY

Gold mineralization at San Luis occurs as tabular ore bodies within and below a low-angle fault zone in cataclastically deformed and metamorphosed Precambrian rocks. The hanging wall is represented by Precambrian metamorphic rocks which are cataclastically deformed and by Tertiary-Quaternary sediments which are interbedded with minor volcanic flows (figs. 3 & 4).

Precambrian rocks

Precambrian, biotite gneiss (1800-1700 Ma; Tweto, 1979) and gneissic granite (1400 Ma; Tweto, 1979) are the dominant basement lithologies at the mine. The altered biotite gneiss unit is the host of gold mineralization (figs. 3 & 4).

Biotite gneiss

Biotite gneiss is a gray quartz-feldspar-biotite gneiss, predominantly occurring below the low-angle fault zone (figs. 3 & 4). The rocks are medium to fine grained, structurally deformed and hydrothermally altered. Gneissic foliations are well developed and change from east-west, 15° to 25° in the

east ore zone, to north-south, 15° to 25° west in the northwestern part of the west ore zone. These foliations are found to have the same orientation as the low-angle fault up to 80 m below the clay zone. Modal composition of the biotite gneiss near ore mineralization is 25 to 35% quartz and 5 to 10% biotite. The remaining amounts is represented by altered minerals sericite, chlorite, specularite, magnetite and hornblende.

Gneissic granite

Gneissic granite is a 1700 Ma (Tweto, 1979) gray to reddish-gray quartz-orthoclase granite, and is the dominant hanging wall lithology of the fault zone. Gneissic granite outcrops in the northern part of the west ore zone, where it is locally crosscut by pegmetites of potassium feldspar and quartz. Primary metamorphic foliations are obscured by a northwestern trending cataclastic deformation related to movement along the low-angle fault zone. Modal composition is 30 to 35% orthoclase and 25% quartz, the remaining consists of muscovite, biotite, amphibole, chlorite, clay, sericite and iron oxides. Gneissic granite is not known to host gold mineralization.

Tertiary igneous rocks

Tertiary igneous rocks include volumetrically significant felsite dikes and andesite dikes and flows.

Felsite dikes

Felsite dikes are pale green to gray intrusive rhyolite, trending N to NNW. The texture is aphanitic to weakly porphyritic, with the presence of quartz and euhedral feldspar megacrysts upto 52 mm in dimension. The thickness of the dikes do not exceed 10 m and they are pervasively sericitized, and weakly to strongly silicified. K/Ar dates on sericite from two pervasively alterd felsite dikes are 24 ± 1 Ma and 24.1 ± 11 Ma (K/Ar; Krueger Geochron Laboratories).

Andesite dikes and flows

Andesite dikes apparently cross cut all rock types excepts Santa Fe formation and younger sediments, and typically trend N-S. Pyroxene, plagioclase, biotite, hornblende and magnetite are present in the dikes (De Ruyter, 1988). Andesite flows occur in the southern part of the mine area, and they interbed with Santa Fe sediments. The Andesite is believed to be younger

than 24 Ma.

Figure 3. Representative Cross-section of the East Ore Zone, rock types same as Figure 2.

Figure 4. Representative Cross-section of the West Ore Zone, rock types same as Figure 2.

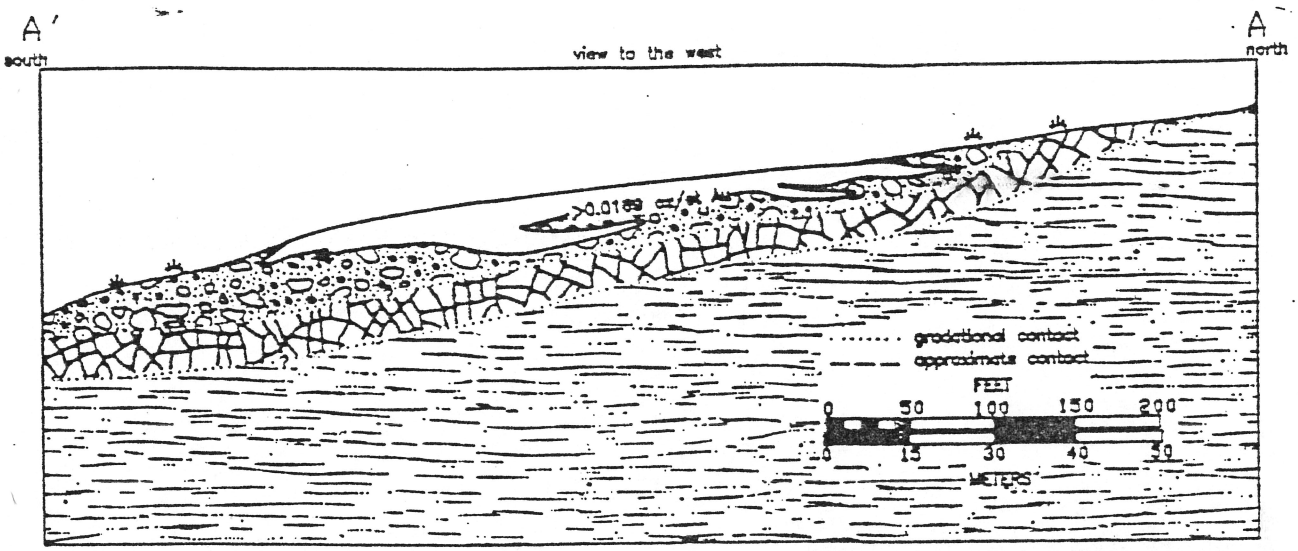
A'
south
view to the west
A
north
>0.0169 oz/yd³ Au
gradational contact
approximate contact
FEET
0 50 100 150 200
0 15 30 40 50
METERS

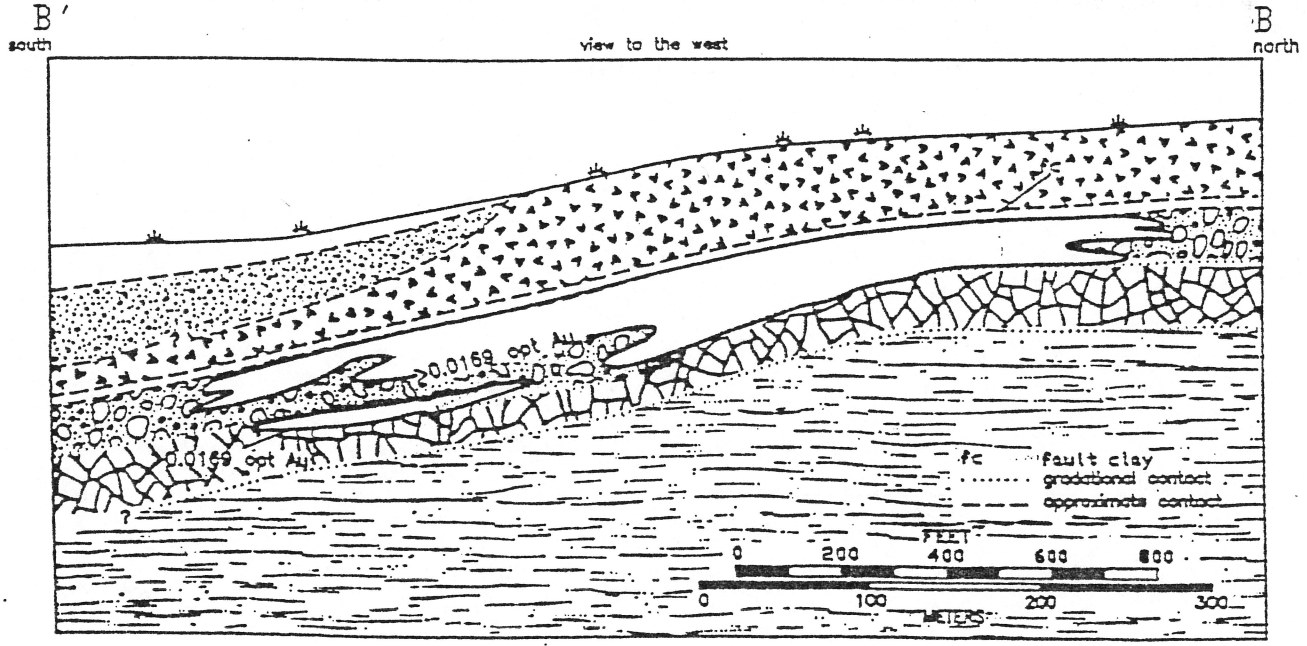
B'
south
view to the west
B
north
>0.0169 opt Au
>0.0169 opt Au
?
fc
fault clay
gradational contact
approximate contact
FEET
0 200 400 600 800
0 100 200 300
METERS

Tertiary-Quaternary sedimentary rocks

Tertiary Santa Fe Group overlies directly gneissic granite in the west ore zone and biotite gneiss in the east ore zone. It consists of silts, sands, gravels and cobble lenses in repetitive sequence.

Quaternary alluvium consists of sands and channel-filling gravels.

STRUCTURAL GEOLOGY

The principal structural feature of the San Luis deposit is the low-angle normal fault zone separating footwall biotite gneiss from hanging wall gneissic granite (fig. 2). The fault caps the west ore zone and has been eroded from the east ore zone. The strike of the fault changes from W-NW in the southern mine area to north in the northern mine area. The fault dips 15° to 25° to the S and SW(fig. 2). Based on interpretations of slickenside features, strikes and dips of hanging wall foliations, and the apparent northeastward rotation of beds and flows in the Santa Fe Formation, the movement on the fault is inferred to be down-dip to the south and southwest.

The faulting was at least in part syn-mineralization which is indicated by the presence of non-disturbed, folded and brecciated quartz veins in single outcrops. Three structural lithologic units were defined on the basis of the low-angle fault zone by Benson and Jones:

(1) fault clay zone of 2-3 m in thickness separating gneissic granite from the underlying biotite gneiss. It is locally silicified, and its color ranges from gray to gray green to pale reddish brown. This zone is unmineralized and probably formed through extreme grain size reduction of the gneissic granite during displacement along the low-angle fault.

(2) Biotite gneiss breccia, which hosts more than 80 percent of the ore, consists of sub angular to subrounded quartz and lesser amounts of feldspar ranging in size from ⟨ 1mm to 10's mm, set in a fine-grained rock flour matrix.

(3) Biotite gneiss cataclasite, consisting of sub angular to subrounded rock fragments in a weakly foliated fine-grained rock flour matrix.

Numerous north-south striking, steeply dipping faults occur in the vicinity of the deposit. The west ore zone is partially cut off on the north by a steeply-dipping, east-west striking fault. A steeply-dipping east-northeast striking fault partially cuts off the east ore zone. West of the deposit is inferred north-south striking normal faults which probably down drop basement and sedimentary rocks hundreds to thousands of meters to the west (Benson and Jones unpublished paper 1991).

METHODS OF INVESTIGATION

Two weeks were spent on field studies to understand the geology and the relations between the various rock units of the Complex. Special emphasis was put on the description of physical features such as the nature of mineralization, structural controls, alteration and paragenesis. Samples were collected for petrographic and geochemical studies.

Sampling was done on two transversal lines to the ore body, in order to study the petrographic and geochemical changes in the mine area. One line was across the east ore zone and at a direction of 10 NNW. The second was east west across the west ore zone. Samples of one to three kilograms in weight were collected from outcrops of different rock units. Thirty samples were selected on the basis of megascopic petrology and were sent to Gold Hill Geological Research Company in Albuquerque, New Mexico for thin and polished sections preparation. These were analyzed under transmitted and reflected light microscope. Chemical analyses of eighteen samples of various rock units occuring in the mine area were done by standard geochemical methods at XRAL Activation Services Inc., Michigan. Samples were analyzed for SiO_2, Al_2O_3, CaO, MgO, Na_2O, K_2O, Fe_2O_3, MnO, Cr_2O_3, P_2O_5, TiO_2 and loss on ignition. Trace elements Ba, Nb, Rb, Sr, Y and Zr were analyzed by x-ray fluorescence spectrometry on a fused disc prepared from the sample. Cu, Pb, Zn and S were analyzed by XRF and were determined as total concentrations

using the pressed pellet technique, avoiding potential dissolution problems.Instrumental neutron activation method was used for the analyses of Au and Cr.

Ten samples were analyzed for clay minerals by a Rigaku diffractometer. All x-ray patterns were obtained using CuKγ radiation, a curved crystal monochrometer, at a scanning speed of two degrees 2α per minute, a chart speed of one inch per minute, and slit size of 1-3-1.

Mineralogy as inferred from thin and polished section studies and x-ray diffraction results were used to define the type of alteration, mineral assemblages and zonation. Major and trace elements were used to understand chemically the alteration and to determine the correlations of various compounds.

Fluid inclusion microthermometry analyses were carried out on ten samples of quartz from highly altered and less altered rocks. Doubly polished quartz slices were prepared for heating and freezing stage studies. The calibration of Linkam TH 600 stage was checked using the provided water and carbondioxide standards at New Mexico Tech fluid inclusion laboratory, and the corrections were made. The Linkam TH 600 stage was used to infer conditions during mineralization such as temperature and salinities of the mineralizing fluid.

Gas analyses from primary and secondary fluid inclusions in quartz were obtained by using methods described in Norman and Sawkins (1987). The same samples used for fluid inclusion microthermometry analyses were also

used for these bulk analyses. The rock samples were crushed and -10/+30 mesh size froctions were seperated. A sample is placed in a beaker containing warm 10% NaOH for about 15 minutes, then washed in distilled-deionized water. The sample is placed in 50% analytical grade HCl and 50% distilled-deionized water for about 15 minutes to remove any contamination from the surface of the grains. The sample is rinsed in distilled-deionized water, then boiled in distilled water for 24 hours. The sample is dried in an oven at a temperature of 60° c. Samples of about 1 to 5 gms each are placed in the quartz furnaces. Rough vacuum was applied to samples followed by high vacuum. In order to remove any absorbed components on the samples, they are heated in vacuum overnight at a temperature of 100° c , until a pressure of 4×10^{-7}m bar was attained. The samples were heated to 500° c for 15 minutes to decripitate the fluid inclusions in the quartz material. The released volatiles were seperated into condensable gases (CO_2, H_2S, SO_2 and C_nH_n hydrocarbons) trapped with a liquid nitrogen bath and non condensible gases (H_2, N_2, CO, CH_4, He and Ar) trapped with dry-ice alcohol filled Dewar. Non condensable and condensable gases are entered seperately into the quadrupole mass spectrometer. The quantitative analysis was computed from the mass spectra, and the total moles of the gases were calculated by computer using the amount of gas, pressure and volume of the extraction line. Water was measured by pressure measurement. The total gas value includes the non condensable, condensable and water phases.

DATA

MINERALIZATION AND ALTERATION

The main expression of hydrothermal activity in the district is the presence of large volumes of altered rocks. The alteration products were studied and defined megascopically in the field and later examined and characterized by petrographic microscope and x-ray diffraction methods. The alteration zones within the rock types were classified according to diagnostic mineral assemblages and textures. In thin sections, the prevailent style of alteration observed is primary quartz, microcline and plagioclase are partially to totally replaced by fine-grained sericite (illite) and carbonate, biotite is replaced by chlorite.

MINERAL ASSEMBLAGES AND ALTERATION ZONES

The altered rocks display a sericitic, intermediate argillic and propylitic alteration zones (fig. 5). The zone boundaries are not sharp but rather grade into the next, making it difficult to map boundaries.

Sericitic alteration

This phyllic alteration is the most important, type in the deposit, it shows

a close association with gold occurring in close association with ore. This zone can be divided into two subzones, which are typified by high silicification and a subzone where early hematite-specularite is the dominant alteration that was overprinted by silica and sericite mineralization. The characteristic mineral assemblage of sericitic alteration is: quartz - sericite - pyrite ± hematite-specularite ± galena ± K-feldspar ± calcite ± chlorite.

Weak / Intermediate argillic alteration

Intermediate argillic alteration consists of weakly developed illite (sericite) and minor amounts of kaolinite. It forms a distinct zone around quartz-sericite-pyrite zone and contains very few to no sulfide minerals. This zone is characterized by an assemblage of quartz-sericite ± kaolinite ± K-feldspar ± calcite ± chlorite ± magnetite.

Propylitic alteration

The propylitic alteration is found peripheral to the deposit and consists of less intense alteration assemblage of chlorite - calcite - albite ± sericite ± quartz ± K-feldspar.

Figure 5. Schematic of Alteration Zones

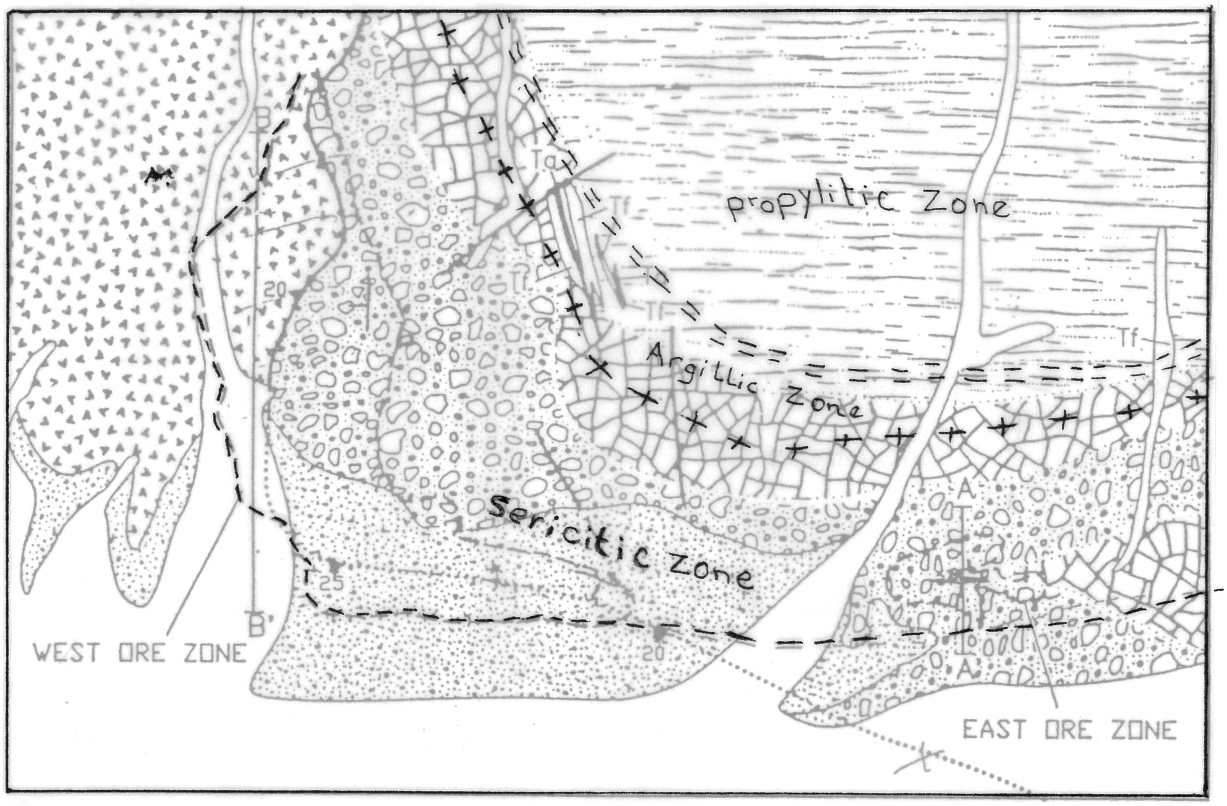

N

0 1000 FEET 2000 3000

0 1 2 3 4

KILOMETERS

LOCATION OF MAP AREA

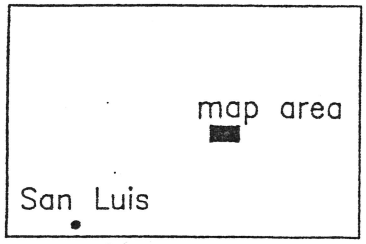

Tertiary
- alluvium
- Santa Fe Formation
- Ta andesite
- Tf felsite

Precambrian
- biotite gneiss breccia
- biotite gneiss cataclasite
- gneissic granite
- biotite gneiss

- faults (dotted where inferred)
- surface projection of ore contours (>0.0169 oz/st Au)
- detachment fault, teeth on hanging wall (dotted where inferred)

ALTERATION MINERALS

Clay minerals are the dominant alteration mineral found in the San Luis mine. The principal types of clay minerals are illite and chlorite. In addition minor amounts of smectite, mixed-layer of illite-smectite and kaolinite have been detected by XRD analysis. The clays occur in veinlets accompanied by quartz, calcite, pyrite and/or K-feldspars as well as massive replacement of plagioclase and biotite.

Illite (sericite)

Illite is a significant alteration clay mineral in the district. Illite occupies dissolution cavities in primary feldspar, as inclusions in quartz, in pore spaces in the ground mass and as fracture fillings. It is the dominant alteration mineral within quartz-sericite-pyrite alteration halo that envelopes the mineralization. It decreases in amount with increasing distance outward from the ore body.

Smectite, illite-smectite mixed-layer

Smectite and illite-smectite mixed-layer clays were identified by x-ray diffraction. They occur in minor amounts. Smectite and illite-smectite mixed-layer are present in the illite-chlorite-calcite zone.

Chlorite

Chlorite is a common alteration mineral filling pore spaces in the groundmass, lining vugs and filling fractures. Its color is green and show very weak pleochroism and moderate birefrengence. The grain size ranges from < 0.03 to 0.07 mm. Chlorite occurs as a significant alteration product within the Illite-chlorite-calcite zone. It occurs generally with illite and calcite.

Albite and K-feldspar

K-feldspar occurs as disseminated grains in the ground mass and as fracture fillings in all rock types but at different proportions. K-feldspar grain size varies from < 0.06 to 0.5 mm. Albite was indicated by XRD analyses, and was not observed in thin section. It may be an alteration product of plagioclase. Albite and K-feldspar are in common association with chlorite and calcite.

Calcite

Calcite is formed throughout the altered rocks as replacements of ground mass of all rock types and plagioclase phenocrysts in biotite gneiss rocks. It also occurs as veinlets and fills cavities, vugs and fractures.

Silica minerals

The principal silica mineral observed in the mine is quartz. Quartz is by far the most abundant mineral occurring with varying amounts of sericite (illite), calcite, chlorite, K-feldspar and pyrite. It forms veinlets and occurs as subrounded particles in the ground mass of all rocks.

ORE MINERALOGY AND PARAGENESIS

Under the microscope and at hand specimen of sericitically altered rock the principal sulfide mineral present is pyrite, with moderate to minor occurrence of chalcopyrite and galena. Specularite, hematite and chlorite are associated with less intense hydrothermal alteration. Pyrite is the most abundant mineral followed by in order of deceasing occurrence by chalcopyrite, hematite and minor amount of galena. Ore microscopy studies of sulfide concentrates done by Schurer and Fucho (1988) (Benson 1991), indicate the presence, in order of decreasing abundance, of pyrite, chalcopyrite, hematite, goethite, anatase, galena, molybdenite, covellite, gold and pyrrhotite. However, neither goethite, anatase, molybdenite, covellite or pyrrhotite were observed in the mine area, or in the polished section during this study. Fluorite is reportedly present in narrow quartz-fluorite veinlets and in open-space filling (Benson 1991). This was observed in several samples displayed by Benson, but not in the field. Gold about 20 microns in dimension, is reported to occur along fractures in pyrite grains, as small blebs within pyrite grains and as discrete particles mainly electrum (Benson 1991). No gold particles were observed during this study in thin or polished sections. Ore associated gangue minerals includes quartz, sericite, calcite, dolomite, specularite and muscovite.

MINERALIZATION

Pyrite

Pyrite is the most abundant sulfide in the district. It is generally euhedral to subhedral in form. Fragmented grains are also found. Pyrite occurs in veinlets and as disseminations. Benson (1991) defined three forms of pyrite in the mineralized zones: euhedral, untarnished and relatively coarse-grained pyrite that has little correlation with gold mineralization; untarnished, poorly-twined pyritohedrons that has little or no correlation with gold mineralization; and irregular fine-grained clots of tarnished pyrite that appears to have the most consistent correlation with gold mineralization. It was impossible to differentiate the three types of pyrite described above in polished section. This may be due to sample preparation, which removes tarnish. However, no clear relationship between pyrite grain-size, shape, and occurrence near ore zone. The number of samples studied was small, and Benson's observations may best be seen in the field.

Chalcopyrite

Chalcopyrite is the second most abundant sulfide in the mine. It is generally coarse-grained and occurs mostly in contact with pyrite grains.

Chalcopyrite was observed commonly replacing pyrite.

Galena

Galena occurs as sub angular grains and shows fracturing to some extent. Galena is generally interstitial to quartz and was observed within the ore body.

Hematite-Specularite

Hematite-Specularite is generally interstitial to quartz, also occurs in fractures, as well as disseminations. The hematite-specularite grains are commonly sub angular to subrounded in form.

PARAGENESIS

There is only evidence for one stage of mineralization (fig. 6). There is no contact between the east ore zone and west ore zone, however the two ore bodies are assumed to be contemporaneous on the basis of their similar mineralogy and textural patterns. In both ore bodies, quartz is early, sericite occurs as flakes on quartz, it is the second deposited mineral after quartz. K-feldspar appears to be in textural equilibrium with early quartz. Pyrite occurs

after quartz and is associated with galena that appears to be deposited at the same time. Chalcopyrite occurs as replacement of pyrite. Some sericite appears to be after plagioclase. Specularite-hematite occurs as a later phase and is overprinted by later silicification and sericitization, there is also evidence that hematite-specularite was deposited before and during deposition of pyrite. Chlorite and calcite veinlets cut all the minerals.

Figure 6. Paragenetic Sequence of Ore Minerals

	TIME OF DEPOSITION
Quartz	———————————————————
Sericite	———————————————————
Pyrite	———————————
Galena	———————————
Chalcopyrite	———————————
K-Feldspar	———
Specu-Hematite	———————————
Chlorite	———————————
Calcite	———————————

GEOCHEMISTRY OF THE ALTERATION AND FLUID INCLUSIONS

GEOCHEMISTRY OF ALTERATION

Whole-rock major and trace element analyses of eighteen samples from the two traverses, including altered rock to varying degrees is provided in Table 1 (Appendix I).

The alteration processes that affected rocks hosting the San Luis gold deposit produced significant changes in bulk chemistry (table 1). Chemical analyses plotted on K_2O-Na_2O-CaO, Na_2O-Fe_2O_3-CaO and MgO-Fe_2O_3-Al_2O_3 ternary diagrams (fig. 7), show that samples plot in the K_2O and Fe_2O_3 fields, although relatively unaltered rocks cluster towards the sides of Na_2O-CaO and MgO-Al_2O_3. Figure 8 shows that Al_2O_3 is evenly distributed through the mine area. Table 1, figures 7 and 8 show a relative addition of K_2O, SiO_2 and Fe_2O_3 and correspondingly less Na_2O, CaO and MgO. Although various emperical chemical patterns have emerged, it is impossible to give quantitative estimates for the chemical gains and losses during alteration and mineralization, because fresh rocks are not available for comparison. Hence it is impossible to conclude that potassium in these rocks was introduced by metasomatic phenomena or that the original rocks had a high potassium content or both. Chemical gains and losses must therefore be characterised in an appropriate time frame with the evolution of the mineral assemblages.

The sequence of alteration at San Luis mine, as described above, is characterised by an increase in the proportion of sericite, quartz and pyrite towards the ore body, and a decrease in the proportion of biotite, chlorite and calcite. From the geochemical data provided, it appears that K_2O and Fe_2O_3 increase with the progressive abundance of sericite and pyrite respectively. In the same manner Na_2O, CaO and MgO increase with the occurrence of albite, chlorite and calcite.

The distribution of other elements such as Cu, Pb, Zn and Au shows a spatial distribution. The copper concentration at San Luis mine (fig. 14) is highest (> 873 ppm) within the ore zone in gneiss breccia. In the gneiss cataclasite which has undergone a weak argillic alteration, the values of Cu concentration ranges from 4 to 45 ppm. The copper concentration drops drastically to less than 2 ppm in the biotite gneiss rocks characterised by a propylitic alteration. Large lead concentrations are mostly restricted to biotite gneiss cataclasite near the ore body (fig. 14). Zinc concentrations greater than 65 ppm occur mostly in biotite gneiss breccia (fig. 14). The chemical data for gold, plotted in figure 14, show a high concentration (> 890 ppb) within the biotite gneiss breccia and to a lesser extent in gneiss cataclasite along the ore zone. Gold values decrease away from biotite gneiss unit (ore zone).

Figure 7. Altered and Less Altered Rocks Analyses from San Luis Deposit plotted on a Na_2O-Fe_2O_3-CaO, Na_2O-K_2O-CaO and MgO-Fe_2O_3-Al_2O_3 ternary diagrams

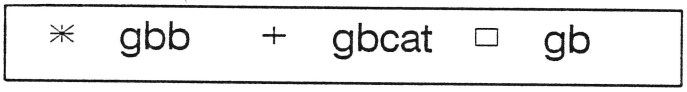

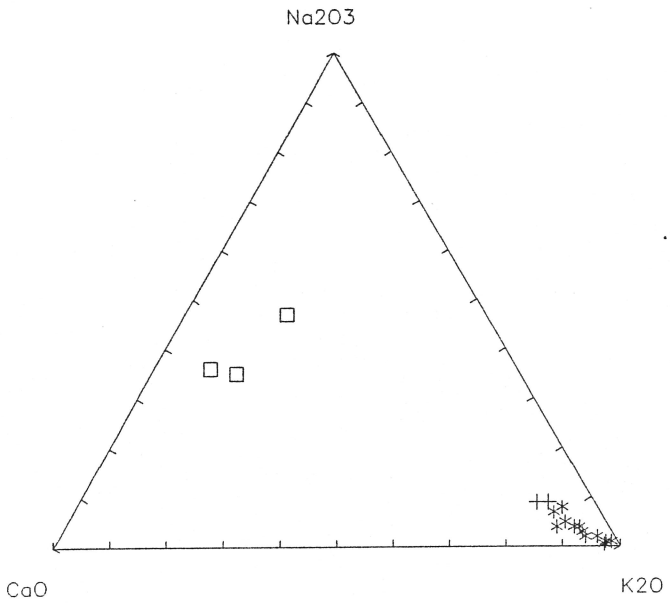
Na2O3
CaO
K2O

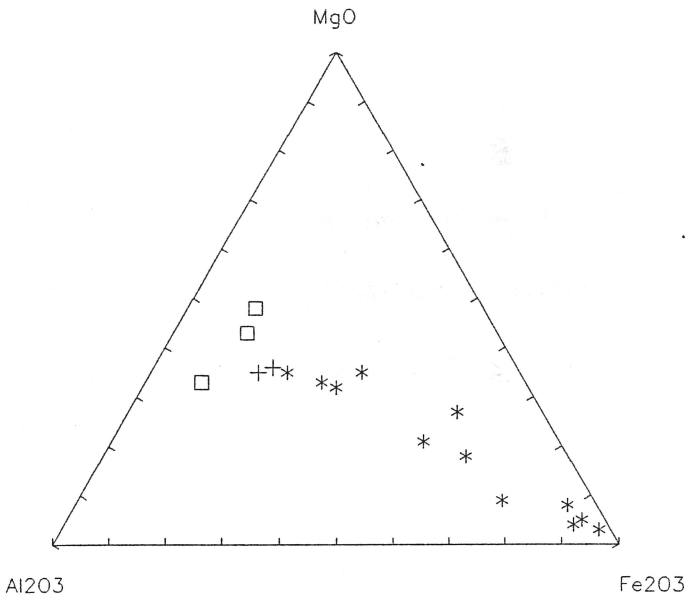
MgO
Al2O3
Fe2O3

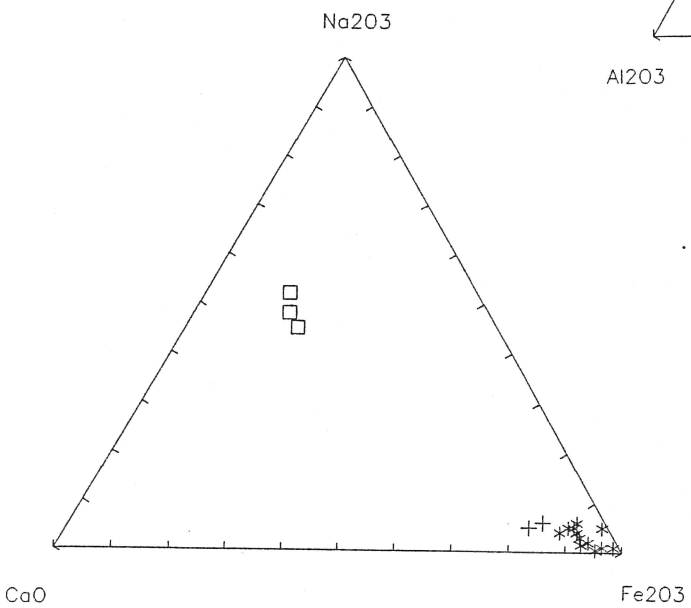
Na2O3
CaO
Fe2O3

Figure 8. Distribution of Al_2O_3 Through the Mine Area of San Luis Deposit

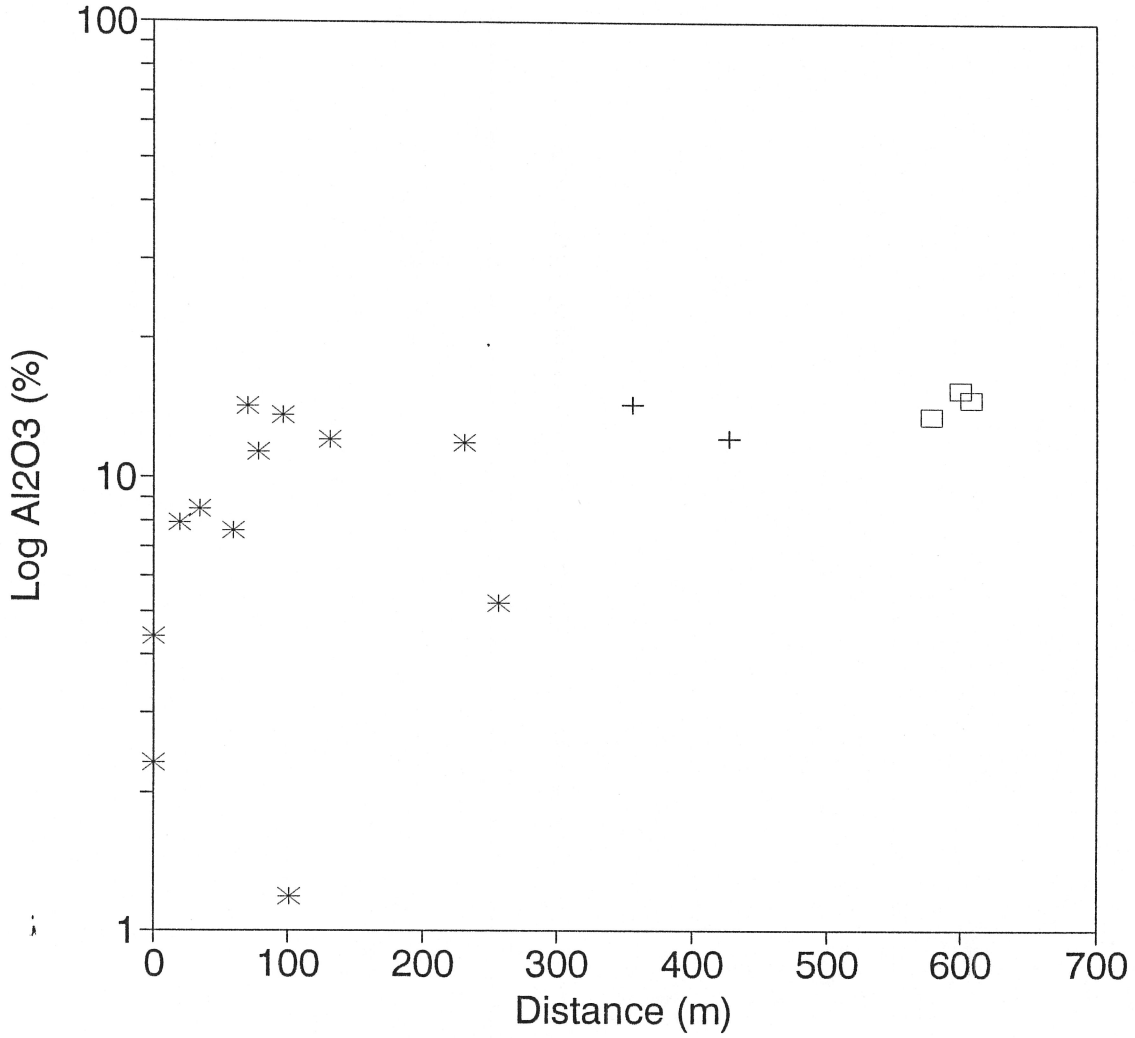
100
10
1
Log Al2O3 (%)
0
100
200
300
400
500
600
700
Distance (m)

Figure 9. Distribution of Fe_2O_3 Through the Mine Area of San Luis Deposit

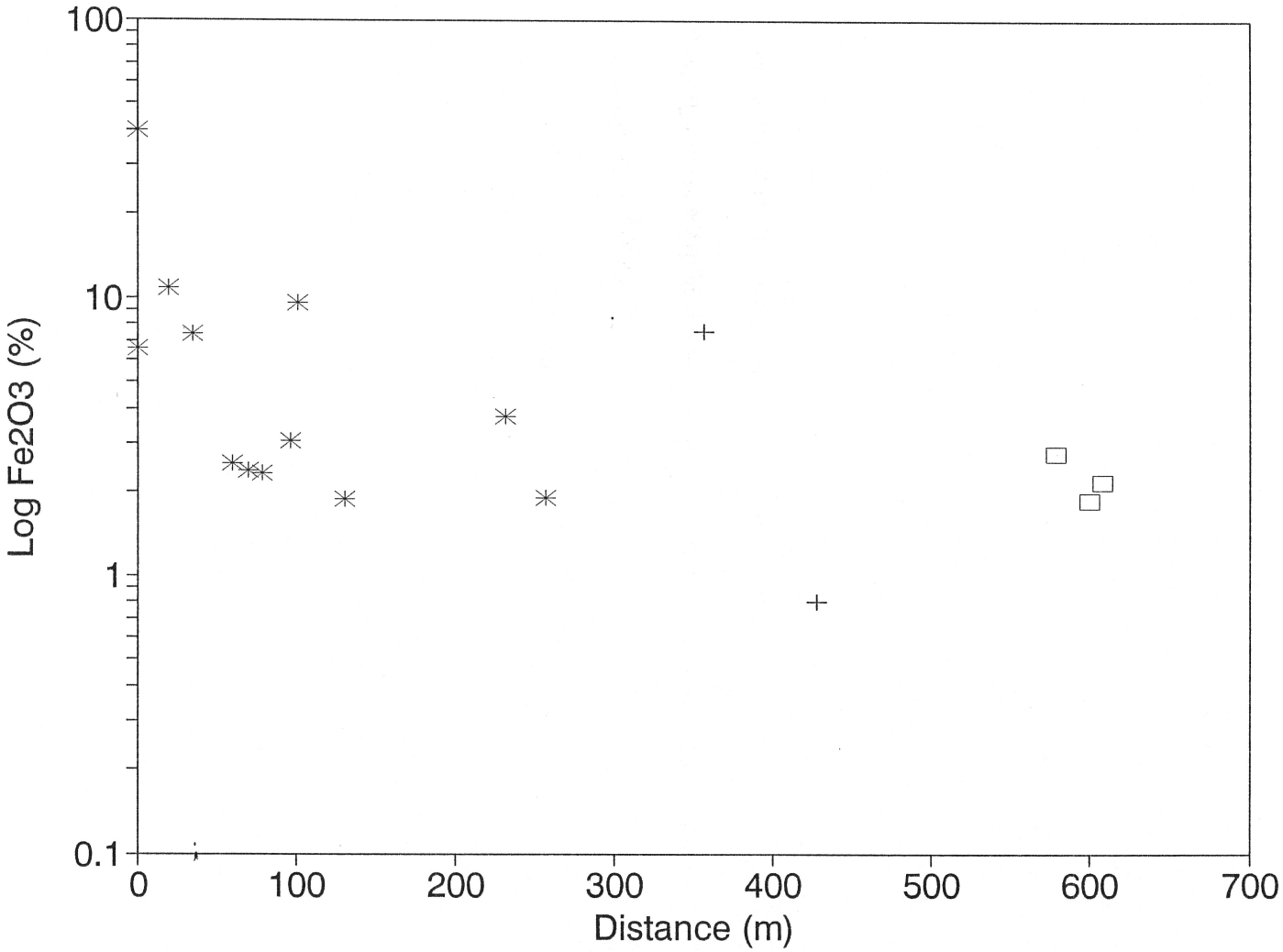
100
10
1
0.1
Log Fe2O3 (%)
0
100
200
300
400
500
600
700
Distance (m)

Figure 10. Distribution of K_2O through the Mine Area of San Luis Deposit

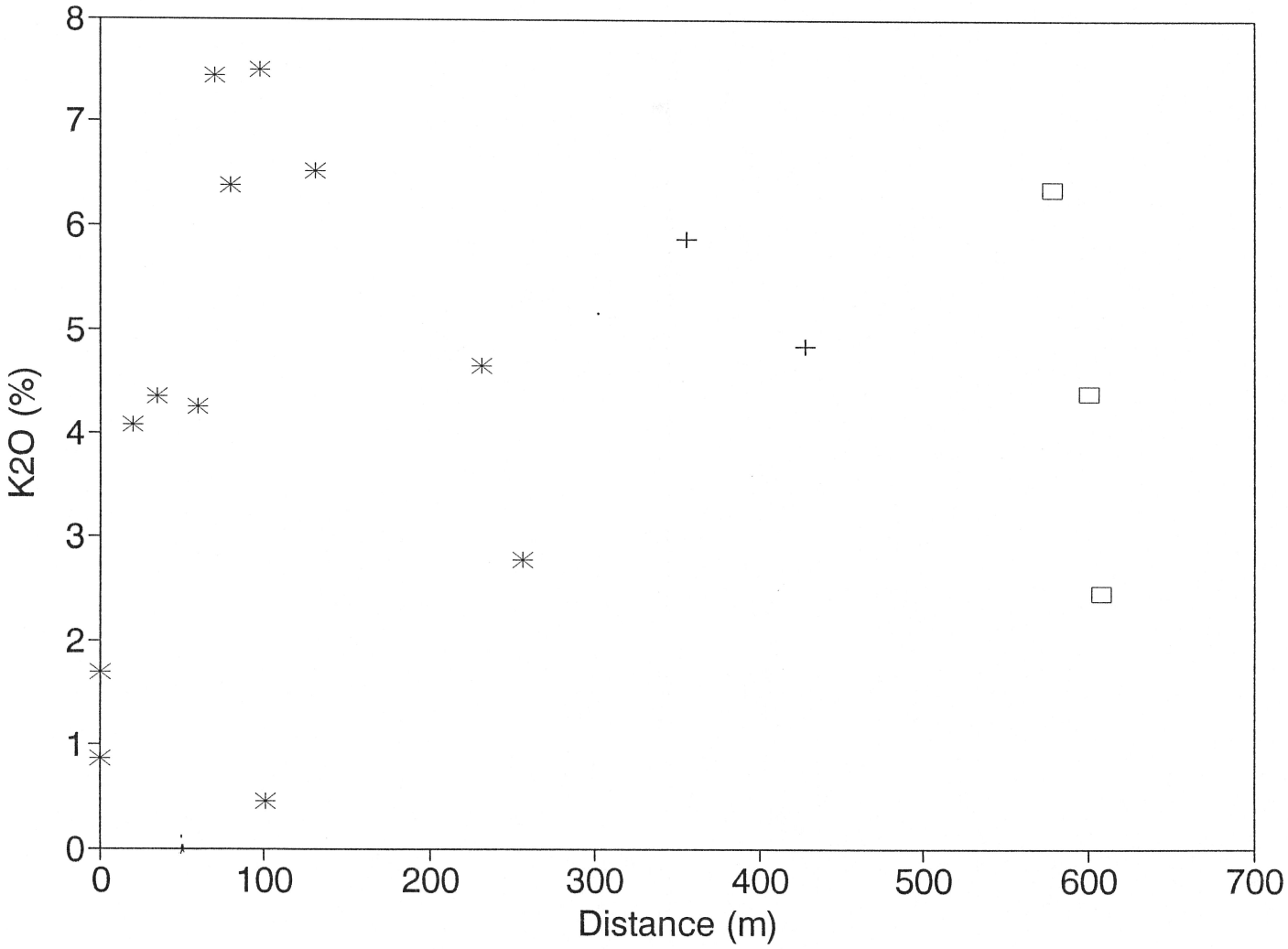
K2O (%)
0
1
2
3
4
5
6
7
8
0
100
200
300
400
500
600
700
Distance (m)

Figure 11. Distribution of Na_2O_3 Through the Mine Area of San Luis Deposit

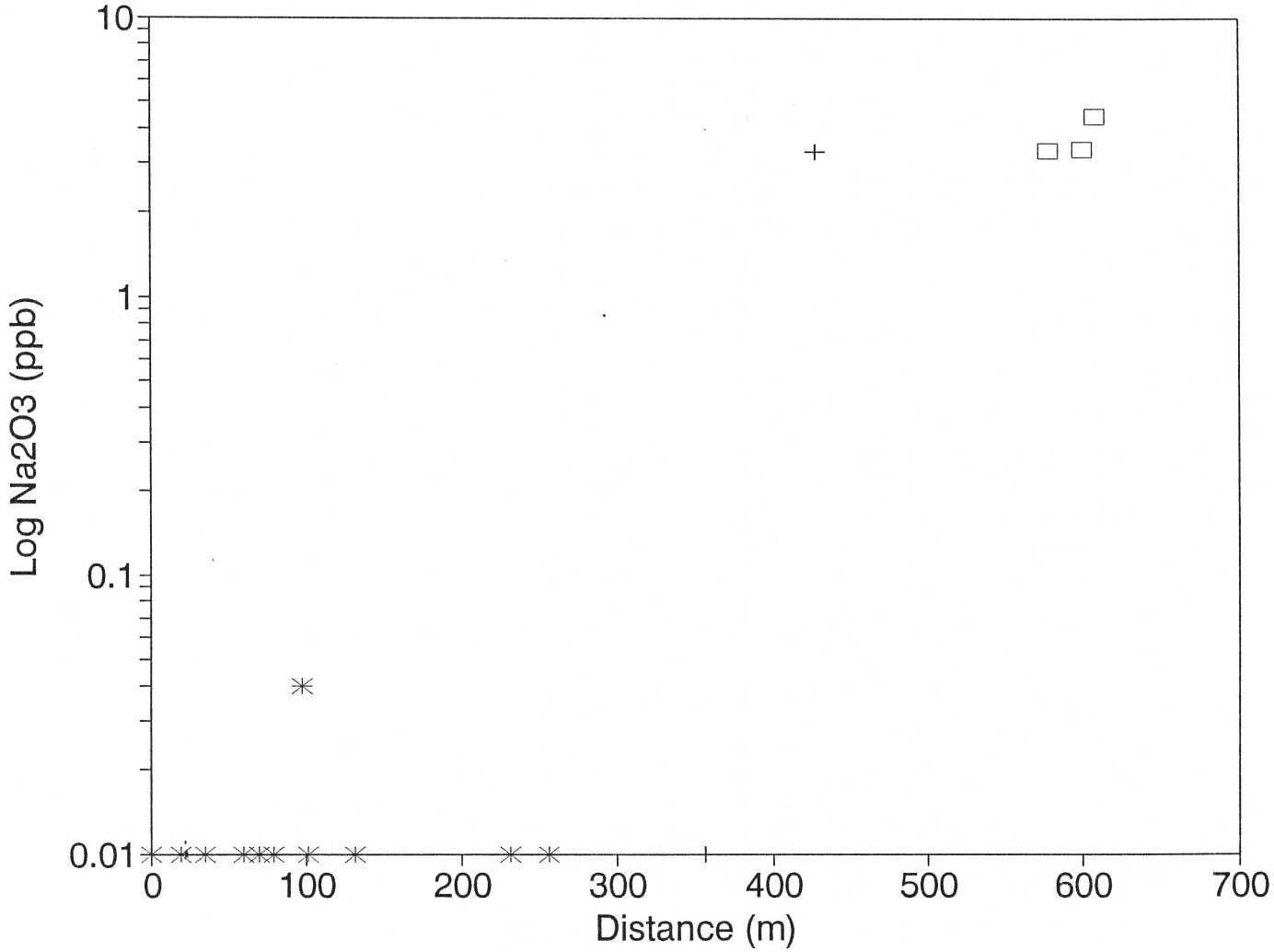
10
1
0.1
0.01
Log Na2O3 (ppb)
0
100
200
300
400
500
600
700
Distance (m)

Figure 12. Distribution of CaO through the Mine Area of San Luis Deposit

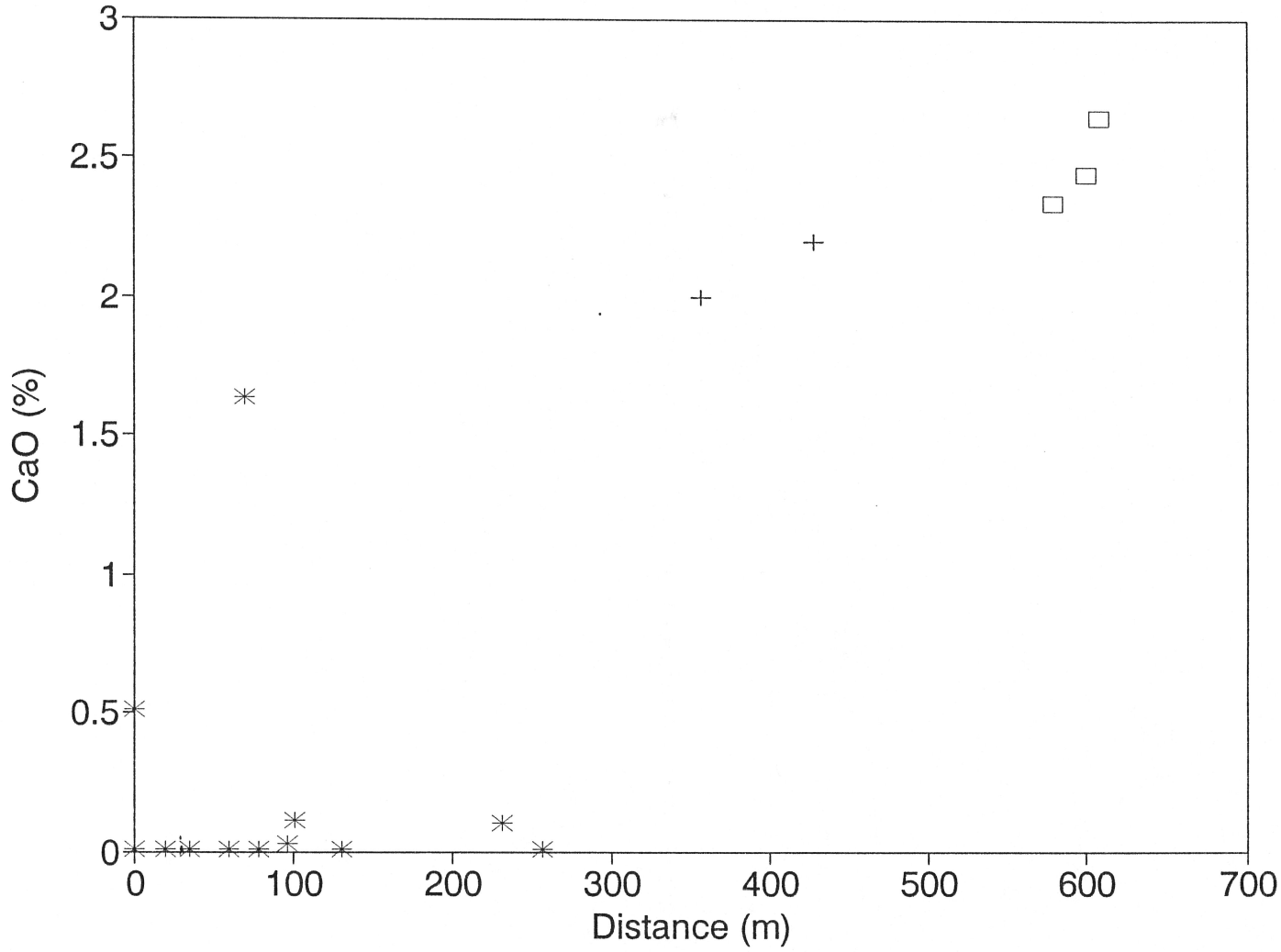
3
2.5
2
1.5
1
0.5
0
CaO (%)
0
100
200
300
400
500
600
700
Distance (m)

Figure 13. Distribution of SiO_2 Through the Mine Area of San Luis Deposit

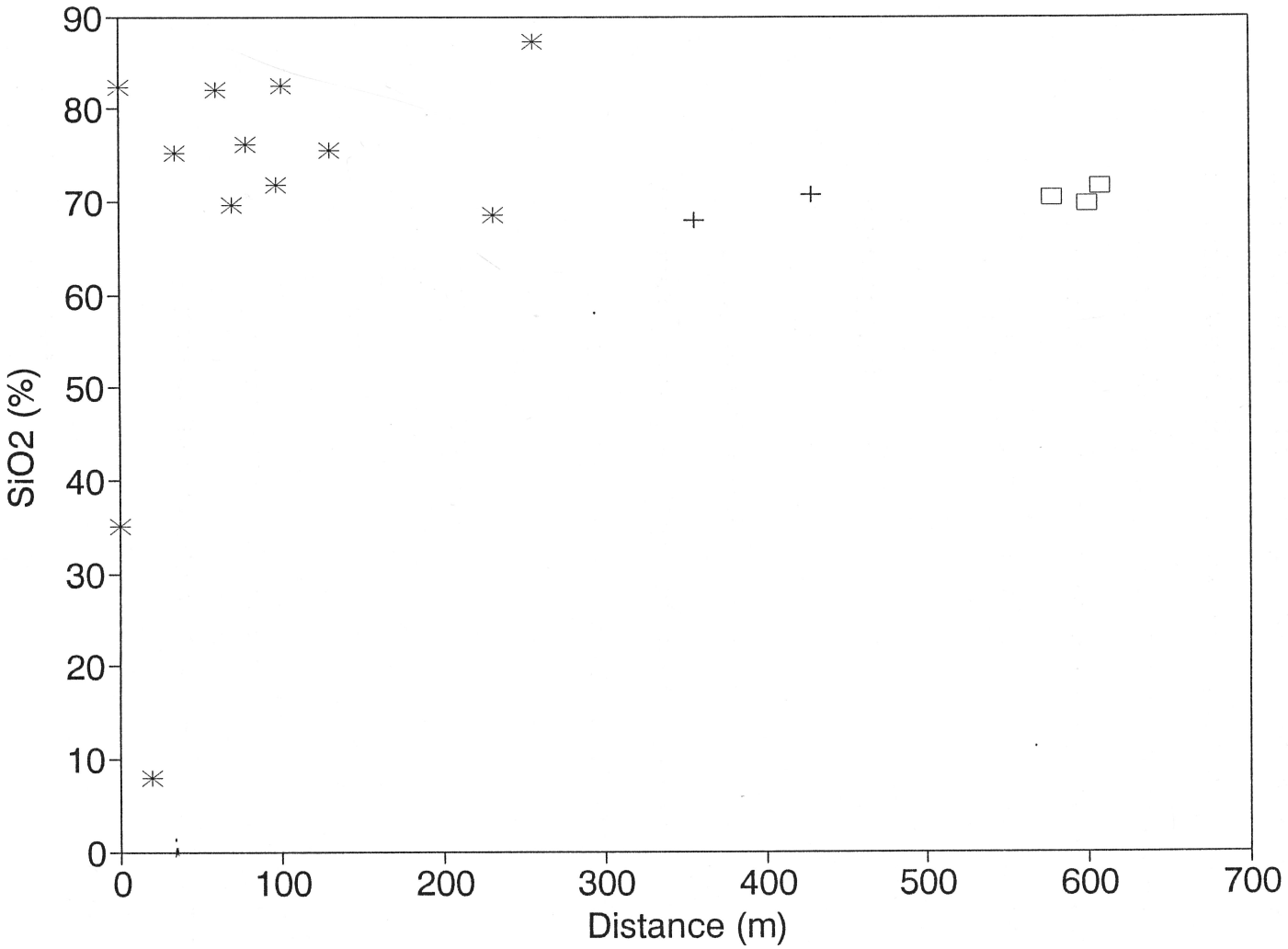
90
80
70
60
50
40
30
20
10
0
SiO2 (%)
0
100
200
300
400
500
600
700
Distance (m)

Figure 14. Distribution of Cu, Pb, Zn and Au Vs. Distance from the Ore at San Luis mine

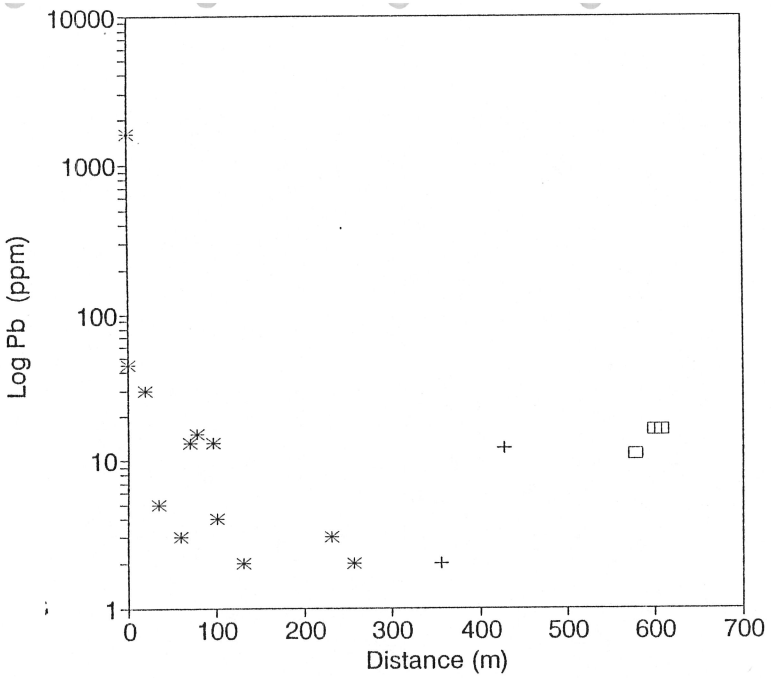
Log Pb (ppm)
10000
1000
100
10
1
0
100
200
300
400
500
600
700
Distance (m)

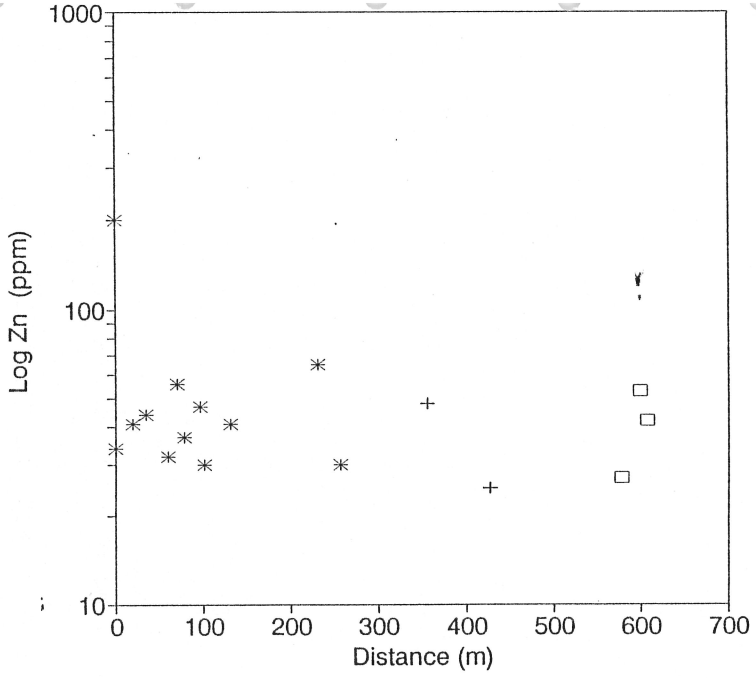
Log Zn (ppm)
1000
100
10
0
100
200
300
400
500
600
700
Distance (m)

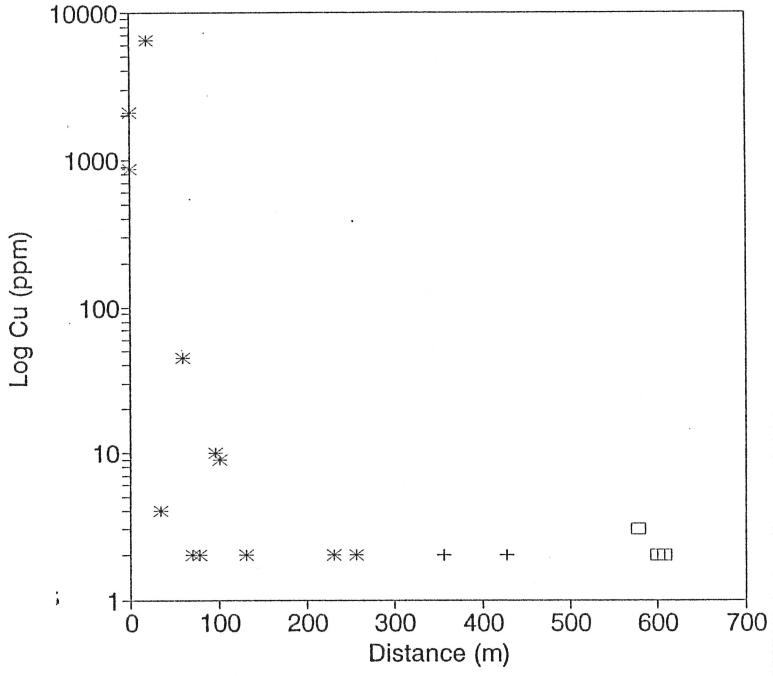
Log Cu (ppm)
10000
1000
100
10
1
0
100
200
300
400
500
600
700
Distance (m)

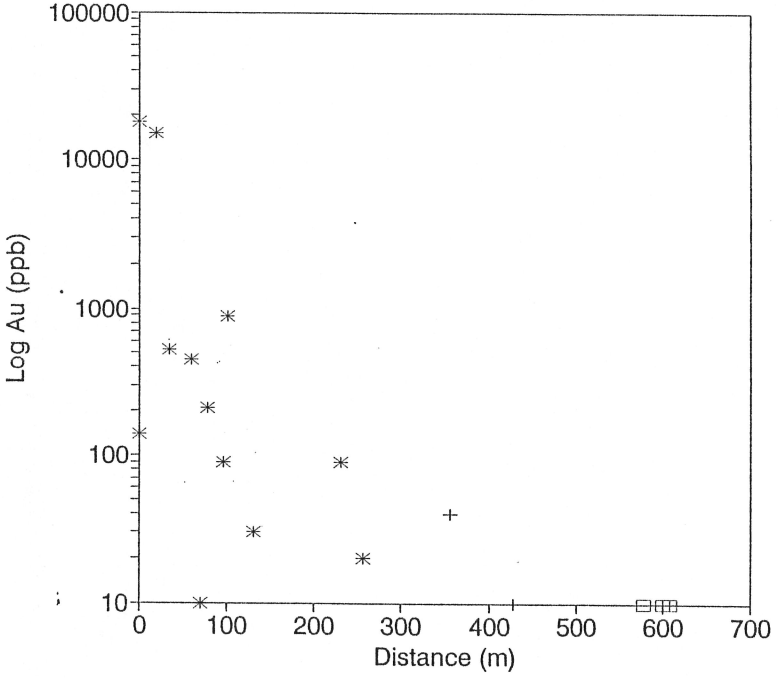
Log Au (ppb)
100000
10000
1000
100
10
0
100
200
300
400
500
600
700
Distance (m)

FLUID INCLUSION STUDIES

The quartz at San Luis provided excellent material for fluid inclusion studies. The principal difficulty was the small size of the fluid inclusions, and the intergrown nature of quartz crystals which makes it difficult to classify fluid inclusions as primary, pseudosecondary, or secondary after multiple intracrystalline deformation and fracturing. Fluid inclusions identified as primary in the San Luis quartz samples are less than 12 microns in diameter and occur as isolated or small clusters of inclusions located randomly within the grains or between healed fractures. Secondary fluid inclusions are smaller in size than primary inclusions, and range to less than 6 microns in diameter. They occur as trials often delineating one or two, some times three, sets of intersecting healed micro fractures. One type of inclusion was distinguished on the basis of their gas-liquid ratios and absence of daughter minerals at room temperature. The type of fluid inclusions defined is two phase, liquid rich inclusions consisting of at least 85 volume percent aqueous liquid and the remaining volume is occupied by a vapor phase. This visual estimate of vapor / liquid ratios, for both primary and secondary fluid inclusions, are reported in Table 2 (Appendix II). Variations in vapor/liquid ratios most likely result from uncertainties associated with estimating vapor/liquid ratios in inclusions with irregular shapes, but could also represent trapping of heterogeneous fluids (Roedder, 1984).

Homogenization data

Homogenization data were obtained using a dual purpose freezing / heating stages. More than 115 inclusions were examined. Seventy five percent of inclusions are primary and twenty five percent were secondary inclusions. All the inclusions are found to homogenize to the liquid phase. Most of primary inclusions homogenized between 200° and 280° c, some homogenized between 160° and 190° c. Secondary inclusions homogenized between 140° and 190° c (fig. 15).

Fluid salinities

Most of the aqueous primary inclusions have salinities in the range of 0 to 6 wt percent NaCl equivalent, usually less than 4 wt percent. Fourteen inclusions have given salinities between 9 and 12 wt percent NaCl. Secondary fluid inclusions have low salinities that range from 0 to 1 wt percent NaCl.

The fluid inclusion salinities are plotted against their corresponding homogenization temperatures in fig. 16. This figure shows secondary fluid inclusions are characterized by low salinities and low homogenization temperatures. The primary fluid inclusions indicates a trend going from fluid characterized by low salinities and high temperatures of homogenization to high salinities and low homogenization temperatures, through inclusions

Figure 15. Histogram for Homogenization Temperatures at San Luis Mine

Figure 16. Salinity Vs. Homogenization Temperatures

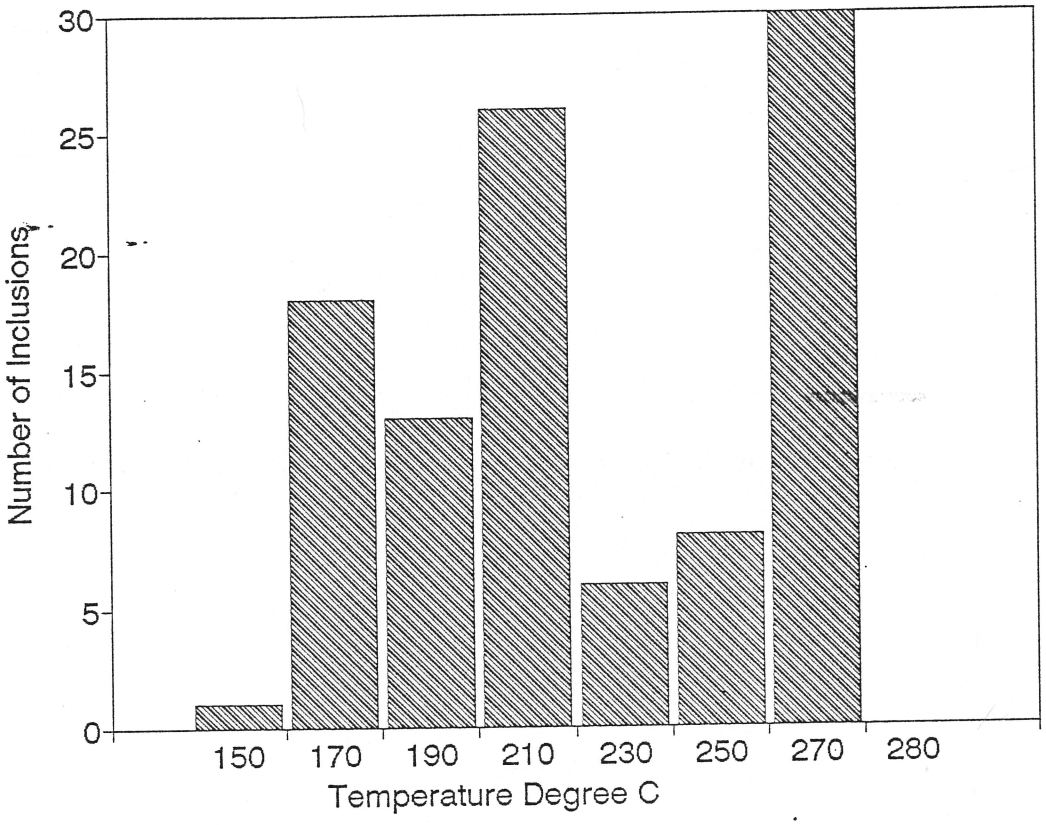

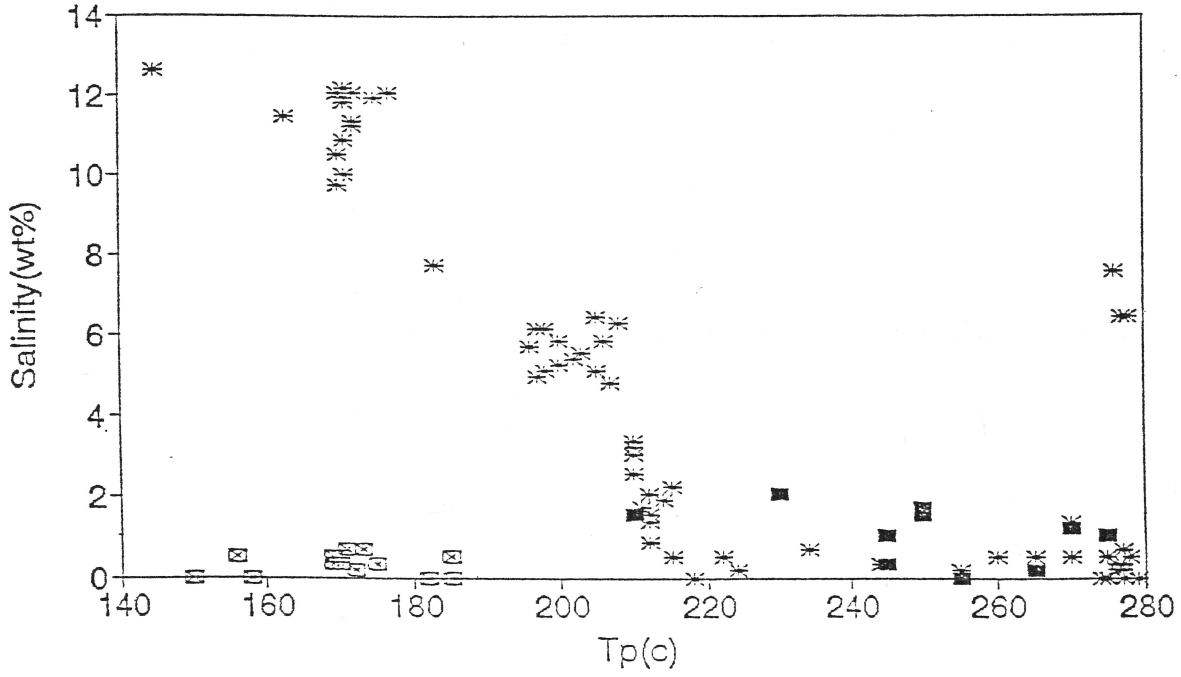

Primary F.I Primary F.I (ore) Secondary F.I

characterized by medium salinities and moderate homogenization temperatures. This may indicate a mixing between high salinity, low temperature fluid with low salinity, high temperature fluid.

GAS ANALYSIS

Quantitative analysis of gases in inclusions was accomplished by using a quadrupole mass spectrometer (Norman and Sawkins, 1987). The fluid inclusions were thermally decripitated at 500° c. The analysis of the volatiles contained in the fluid inclusions are shown in Table 3 (Appendix III). Gas analysis revealed the presence of CO_2, N_2, H_2S, H_2, CH_4, hydrocarbons and H_2O (Table 3). Results indicate that H_2O (64.07 - 94.72 %), CO_2 (1.03 - 25.34 mole %) and H_2S (0.01 - 11.94 mole %) are the dominant gas species. Significant amounts of hydrocarbons, and lesser amounts of CH_4 are revealed. However volatiles in ore samples (KA4, K26) and those close to the ore body (KA27 and KA28B) are generally rich in H_2S (2.52 - 11.94 mole %).

Ternary diagram in the system N_2-H_2-Ar was constructed in order to determine the source of the mineralizing fluid (fig.17). Figure 17 shows that most of the samples cluster between magmatic and meteoric fluid fields. The - N_2-He-Ar ternary diagram compared with the ternary plots (fig. 10) of Norman and Musgrave, 1993, suggests mixing of magmatic water with shallow meteoric water and basin with shallow meteoric water.

Figure 17. Ternary Plot in the System N_2-He-Ar for San Luis Mine

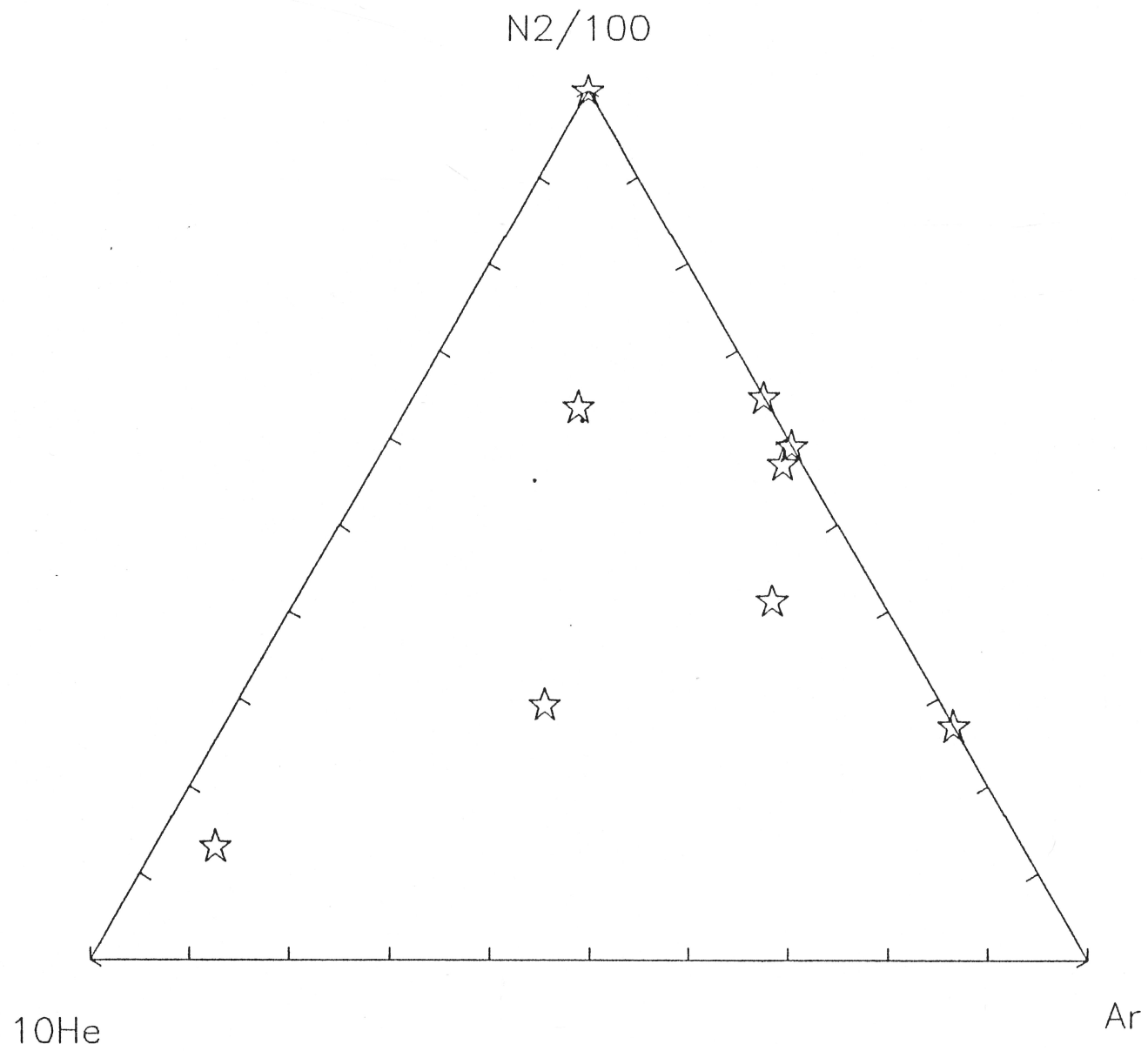
N2/100
10He
Ar

SUMMARY AND DISCUSSION

CLASSIFICATION

Comparision of the San Luis gold deposit with a model epithermal deposit (Guilbert and Park, 1986), and Petorca, central Chile epithermal deposit (Camus. F and et.al., 1991) reveals that San Luis deposit shows most major characterisitcs of epithermal deposits, except that at San Luis the ore occurs as horizontal tabular ore body. The alteration consists mostly of silicification, sericitization, argillization and propylitization. Pyritization is the principal product of mineralization. Ore textures consists of open space filling, brecciation and fine grained material. The mineralization and alteration occurs as thin veinlets, dessimination and replacement. The alteration and mineral zoning were defined in the area, although there is no sharp limit between the zones. The gold mineralization is associated with the sericitic alteration zone which is succeeded by a weak argillic alteration zone outward to the north from the ore body. This is in turn followed by a propylitic alteration which is associated with less altered rocks. Fluid inclusion studies indicate that hydrothermal fluid with temperature ranging from 200° c to 280° c and salinities of 0 to 12 eq. wt. percent NaCl were responsible for ore deposition.

GEOCHEMICAL ENVIRONMENT

The geochemical data shows that the sericitic alteration zone is characterised by a high relative percentage of K_2O, Fe_2O_3 and Al_2O_3, whereas the propylitic alteration zone is depleted in these elements, but characterised by a high relative percentages of Na_2O, Cao, MgO and Al_2O_3. The intermediate argillic alteration is characterised by a moderate percentage of K_2O, MgO, Al_2O_3 and depletion in Na_2O and CaO. The geochemical data shows that SiO_2 is almost evenly distributed through the mine area except in the ore body zone where it is higher and reaches 82.5%. This is reflected in the presence of secondary veinlets and secondary overgrowth of quartz.

The alteration sequence is characterised by an increase in the abundance of sericite, pyrite and a decrease in the occurrence of albite, chlorite and calcite. Na, K, Ca, and Fe gain or loss can monitor the abundance of these minerals. The amount of alkali metals that can be introduced to a rock undergoing alteration is a function of the chemical composition of the original rock. Kerrich and Kyfe (1981), observed that the formation of carbonate minerals in response to introduction of CO_2 from the fluid is largely controlled by the MgO, CaO and FeO contents of the wall rocks. They also concluded that the introduction of K or Na is limited by the availability of Al to form alkali metal silicates.

At San Luis mine it appears that K_2O and Fe_2O_3 increase with the

progressive abundance of sericite and pyrite respectively. In the same manner Na_2O, CaO and MgO increase with occurrence of albite, calcite and chlorite. The alteration patterns and the geochemcial data reveal that the mineralization and the alteration at San Luis mine were formed by a single hydrothermal event. The geochemcial data indicate that there are noticeable differences in the concentrations of some trace elements within and away from the ore zone and that there are distinct differences in the concentrations of some elements between altered and less altered rocks. The figures described previously show that also there is a correlation between Au, Cu, Pb and Zn. Benson (1991) reported that Au correlates with Ag. Therefore the geochemical data for San Luis mine indicate that the gold depositing fluid was part of a polymetallic mineralizing event, and not only reveals a close correlation of hydrothermal alteration with gold anomalies but also indicates that gold is part of a specific alteration assemblage (quartz-sericite-pyrite assemblage).

The fluid inclusion evidence suggests that the gold mineralization stage was not related to boiling processes as has commonly been reported elsewhere for epithermal deposits. Enthalpy versus salinity plots are useful for determining the cooling mechanisms of ascendant hydrothermal fluids (Fournier, 1979). Cooling of the fluid can occur by mixing with cooler, more dilute fluid which decreases both salinity and enthalpy (path OA, fig. 18), boiling which decreases enthalpy but increases salinity (path OC, fig.18),conduction of heat to the host rocks which decreases only the enthalpy (path OB, fig.18), or by

Figure 18. Enthalpy Vs. Salinity for Primary Fluid Inclusions from the San Luis Mine

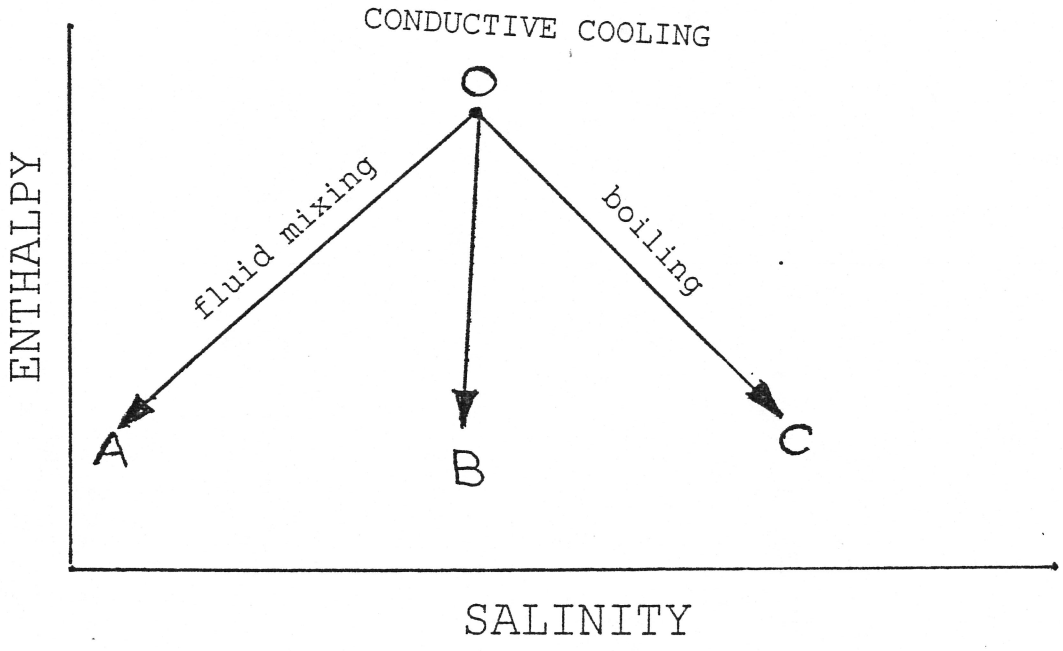
CONDUCTIVE COOLING
O
fluid mixing
boiling
A
B
C
ENTHALPY
SALINITY

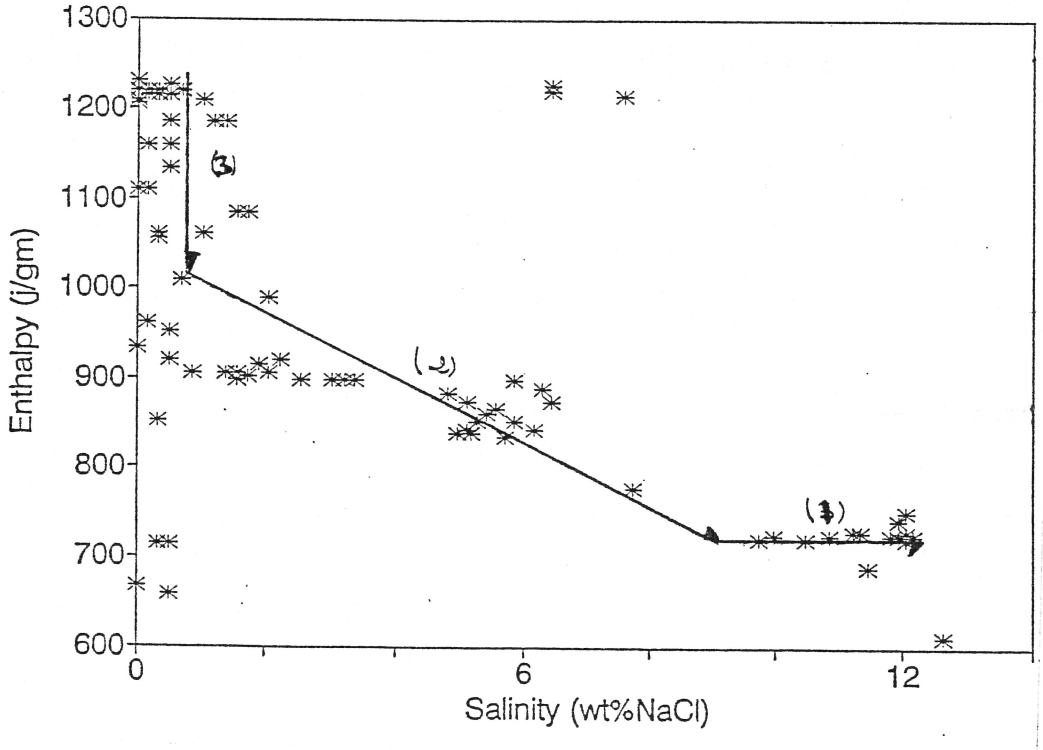
1300
1200
1100
1000
900
800
700
600
Enthalpy (j/gm)
0
6
12
Salinity (wt%NaCl)

a combination of these processes.

For the San Luis area, a plot of enthalpy versus salinity shows three segments: Segment 1 is characterized by constant enthalpy and decreasing salinity. This may be explained by combination of boiling and mixing. Segment 2, indicates decresing enthalpy and increasing salinity which suggest that cooling was caused by mixing and segment three characterized by enthalpy decrease only, this can be explained by conduction of heat to the host rocks.

The N_2-Ar-He gas signature of vapour discharge indicates the sources of these relatively nonreactive gases (Giggenbach, 1986). The N_2-Ar-He composition in fluid inclusions is indicative of of the fluid sources (Norman and Musgrave, 1993). Meteoric ground water that have no other source of these gases preserve atmospheric N_2-Ar ratio even after guetting at depth and heating, though, they may acquire some radiogenic helium and contributions from typical N_2-rich magmatic fluids.

At San Luis deposit the relative N_2, He, Ar contents suggest a significant meteoric water input with a modest contribution from magmatic source. The ratios of these gases, as plotted on the ternary diagram (fig. 17) indicate possibly a mixing of shallow meteoric water and magmatic fluid. The involvement of a deep-circulating water and He-poor shallow meteoric water. The significant amount of hydrocarbons may be indicative of fluid interaction with organic-rich sedimentary rocks. An ore fluid resulting from the mixing of

meteoric water and magmatic fluid is suggested.

The greatest amounts of sulfides and gold occurred in samples associated with high temperatures, high enthalpies and low salinities, where conduction of heat to host rocks is suggested. Gold occurs in fractures in pyrite associated with chalcopyrite and galena. Pyrite and other sulfides probably precipitated as a consequence of the cooling. After the precipitation of pyrite, the hydrothermal fluid would have had a lower H_2S. This would cause the sulfide complexes, which were likely responsible for gold transport (Seward, 1984), in the hydrothermal fluid to become instable resulting in the precipitation of gold. The other factor that controlled the deposition of gold at San Luis mine, besides temperature and chemical changes in the mineralizing fluid, is the structural framework. The gold mineralization at San Luis occurs as tabular bodies and is restricted to the footwall to the low-angle fault zone in cataclastically deformed Precambrian metamorphic rocks. The low-angle fault zone marks the upper extent of the economic mineralization. Therefore the alteration and the mineralization were strongly controlled by this structural fault zone.

The genetic model suggested for the San Luis deposit is as follows :

(1). During the middle Tertiary geothermal gradient along the Rio Grande rift zone, the low-angle detachment fault zone developed and acted as fluid channel and repository for ore deposition.

(2). Felsic intrusions in the form of dike and sills, which may acted as a heat

magmatic volatiles (fluid) and meteoric water.

(3). The hydrothermal fluid responsible for ore transport, which is characterised by high sulfur content, high temperature (up to 280°c) and low salinity (down to 0 eq.wt. % NaCl), cooled and precipitated sulfides resulted in loss of H_2S and deposition of gold.

CONCLUSIONS

1. The alteration at San Luis consists principally of sericitization, silicification and pyritization.

2. The alteration zones were determined to be sericitic zone, which hosts the ore body, followed by intermediate argillic zone and the peripheral propylitic zone.

3. The San Luis deposit is defined to be a low-angle detachment related epithermal deposit, on the basis of the alteration patterns mineralogy and ore textures.

4. The alteration and geochemical data indicate that the mineralization and the alteration were the results of a single hydrothermal event.

5. The metallic elements indicate that the ore bearing fluid at San Luis was a polymetallic hydrothermal fluid.

6. The hydrothermal ore bearing fluid was a mixed magmatic / meteoric fluid. It was a dilute fluid.

7. The low salinity and high sulfur indicate that gold was probably transported as bisulfide complexes.

8. The deposition mechanism probably consisted of cooling which is accompanied with sulfidation, that resulted in loss of H_2S causing the deposition of gold.

REFERENCES

Barns, H. L., Czmanske, G. K., 1967, Solubilities and Transport of Ore Minerals, in Barns, H. L., ed., Geochemistry of Hydrothermal Ore Deposits : New York, Holt, Rinehart, and Winston, p. 334-381.

Barns, H. L., 1979, Solubilities of Ore Minerals, in Barns, H. L., ed., Geochemistry of Hydrothermal Ore Deposits : 2nd ed., John Wiley & Sons, Inc., p. 404-460.

Casadevall, T. and Ohmoto, H., 1977, Sunnside Mine, Eureka Mining District, San Juan County, Colorado : Geochemistry of Gold and Base metal Ore Deposition in a Volcanic Environment : Econ. Geol., v.72, p. 1285-1320.

Ellis, A. J., 1979, Explored Geothermal Systems, in Barns, H. L., ed., Geochemistry of Hydrothermal Ore Deposits : 2nd ed., John Wiley & Sons, Inc., p. 632-683.

Fournier, R. O., 1979, Geochemical and Hydrologic Considerations and the use of Enthalpy - Chloride Diagrams in the Predictions of Underground Conditions in Hot-spring Systems : Jour. of Volc. and Geothermal Research, v. 5, p. 1-16.

Francisco Camus, Ricardo Boric, et. al., 1991, Geologic and Fluid Inclusion Studies of El Brance Epithermal Vein System, Petorca, central Chile : Econ. Geol., v. 86, p. 1317-1345.

Giggenbach, W. F., and R. B. Glover, 1992, Tectonic Regime and Major Processes Governing the Chemistry of Water and Gas Discharges From

the Rotorua Geothermal Field, New Zealand : Geothermics, v. 21, N 1/2, p. 121-140.

Gunther, C. G., The Gold Deposits of Plomo, San Luis park, Colorado : Econ. Geol., v. , p. 143-145.

John, M. Gilbert and Charles, F. Park, Jr., 1986, Alteration Associated with Epithermal Deposits : The Geology of Ore Deposits, p. 196-197.

Kerrich, R., and Kyfe, W. S., 1981, The Gold-Carbonate Association : Source of CO_2 and CO_2 Fixation Reactions in Archean Lode Deposits : Chem. Geol., v. 33, p. 265-290.

Lipman, P. W., Steven, T. A., and Mehnert, H. H., 1970, Volcanic History of the San Juan Mountains, Colorado, as Indicated by Potassium-Argon Dating : Geol. Soc. America Bull., v. 81, p. 2329-2352.

Norman, David, I., and Sawkins, Fredrick J., 1987, Analyses of Volatiles in Fluid Inclusions by Mass Spectrometry : Chem. Geol., v. 61, p. 1-10.

Ogden, T., 1980, Tectonic History of Colorado : Rocky Mountain Association of Geologists, Denver, Colorado, p. 5-9.

Ogden, T., 1968, Geologic Setting and Interrelationships of Mineral Deposits in the Mountain Province of Colorado and South-Central Wyoming : Ore Deposits of the United States, 1933-1967, v. 1, p. 551-582.

Robert, G. B., and David, M.J., 1990, Geology of the San Luis Gold Deposit, Costilla County, Colorado, unpublished company report.

Roedder, E., 1979, Fluid Inclusions as Samples of Ore Fluids : in Barns, H. L., ed., Geochemistry of Hydrothermal Ore Deposits : 2nd ed., John Wiley & Sons, Inc., p. 684-737.

Seward, T. M., 1976, The Stability of Chloride Complexes of Silver in Hydrothermal Solutions up to 350° c : Geochim. Cosmochim. Acta, v. 40, p. 1329-1341.

Seward, T. M., 1984, The Transport and Deposition of Gold in Hydrothermal System, in Foster, R. W., ed., Gold'82 : Rotterdam, Belkema, p. 165-181.

Seward, T. M., 1973, Thio Complexes of Gold and Transport of Gold in Hydrothermal Ore Solutions : Geochim. Cosmochim. Acta, v. 37, p. 379-399.

Shanks, W. C., III, and Bischoff, J. L., 1977, Ore Transport and Deposition in the Red Sea Geothermal System; A Geochemical Model : Geochim. Cosmochim. Acta, v. 41, p. 1505-1519.

Chari, A. K., Charles, E. C., and Jeff, C., 1992, Late Mesozoic to Cenozoic Cooling Histories of the Flanks of The Northern and Central Rio Grande Rift, Colorado and New Mexico : New Mexico Bureau of Mines and Mineral Resources, Bull., 145.

Skinner, B. J., White, D. E., Rose, H. J., and Mays, R. E., 1967, Sulfide Associated with The Salton Sea Geothermal Brine : Econ. Geol., v. 62, p. 316-330.

Weissberg, B. G., Brown, P. R. L., and Seward, T. M., 1979, Ore Metals in Active Geothermal Systems, in Barns, H. L., ed., Geochemistry of Hydrothermal Ore Deposits : 2nd ed., John Wiley & Sons, Inc., p. 738-780.

White, D. E., 1955, Thermal Springs and Epithermal Ore Deposits : Econ. Geol., 50th, Anniv., v. , p. 99-154.

White, D. E., 1974, Diverse Origins of Hydrothermal Fluids : Econ. Geol., v. 69, p. 954-973.

Appendix I : Table 1. Chemical Analyses of Samples from San Luis Mine

	KA1 (gbb)	KA2 (gbb)	KA4 (gbb)	KA6 (gbb)	KA10 (gb)	KA21 (gbb)	KA26 (gbb)	KA30 (gbb)	KA27 (gbb
SiO_2 %	35	69.7	82.5	68.6	70.5	82.4	71	75.2	82.1
Al_2O_3 %	2.33	14.2	1.19	11.9	13.6	4.4	7.9	8.48	7.6
CaO %	0.51	1.63	0.11	5.63	1.34	0.01	<0.01	<0.01	<0.01
MgO %	0.2	0.59	0.09	0.62	0.23	0.28	0.27	0.26	0.24
Na_2O %	<0.01	<0.01	<0.01	<0.01	0.23	<0.01	<0.01	<0.01	<0.01
K_2O %	0.86	7.44	0.44	4.65	6.36	1.7	4.08	4.35	4.26
Fe_2O_3 %	39.8	2.39	9.54	3.77	2.75	6.6	10.8	7.39	2.55
Ba ppm	140	1100	40	530	1800	220	760	710	820
Cr ppm	260	240	510	270	250	100	100	110	150
Cu ppm	2090	<2	9	<2	3	873	6430	4	45
Nb ppm	10	20	10	10	30	30	<10	20	10
Pb ppm	45	13	4	3	11	1600	30	5	3
Rb ppm	50	190	20	150	90	60	90	110	110
S ppm	242000	150	47300	2690	<50	24900	43200	24400	5260
Zn ppm	200	56	30	65	27	34	41	44	32
MnO %	0.02	0.08	0.01	0.27	0.07	0.01	0.01	0.02	0.01
TiO_2 %	0.14	0.33	0.08	0.24	0.33	0.16	0.19	0.29	0.2
P_2O_5 %	0.06	0.09	0.02	0.07	0.08	0.1	0.03	0.07	0.04
Cr_2O_3 %	0.04	0.03	0.08	0.04	0.04	0.01	0.01	0.01	0.02
LOI %	21	1.55	4.85	3.5	0.45	3.9	5.65	4.1	1.75
SUM %	99.99	98.22	98.92	99.4	99.38	99.62	100.1	100.3	98.89
As ppm	43	3	<3	<3	<3	230	<3	<3	<3
Au ppb	140	<10	890	90	<10	18000	15000	530	450
Sr ppm	10	60	<10	60	130	<10	10	20	20
Y ppm	<10	30	<10	20	30	<10	20	20	<10
Zr ppm	50	240	40	170	400	120	220	370	130

	KA23 (gbb)	KA24 (gbb)	KA25 (gbb)	KA16 (gbcat)	KA29 (gbb)	KA18 (gbcat)	KA12 (gb)	KA22 (gb)	KA00 (fd)
SiO_2 %	76.1	71.9	75.6	67.9	87.3	70.8	69.8	71.7	72.4
Al_2O_3 %	11.3	13.6	12	14.3	5.23	12.1	15.5	14.8	15.2
CaO %	<0.01	0.03	<0.01	0.15	<0.01	4.98	1.92	2.64	0.1
MgO %	0.32	0.4	0.31	0.63	0.17	0.25	0.53	.76	0.74
Na_2O %	<0.01	0.04	0.01	<0.01	<0.01	3.3	3.38	4.46	<0.01
K_2O %	6.38	7.5	6.52	5.88	2.79	4.84	4.39	2.47	5.78
Fe_2O_3 %	2.33	3.08	1.88	7.59	1.92	0.8	1.86	2.18	2.3
Ba ppm	1100	1600	750	730	490	500	1200	1100	540
Cr ppm	110	60	90	200	120	260	160	260	50
Cu ppm	<2	10	<2	<2	<2	<2	<2	2	62
Nb ppm	20	20	<10	30	20	10	20	20	30
Pb ppm	15	13	<2	2	<2	12	16	16	200
Rb ppm	150	170	170	170	80	100	100	60	200
S ppm	2330	620	550	1250	3990	<50	<50	<50	<50
Zn ppm	37	47	41	48	30	25	53	42	71
MnO %	0.02	0.02	0.02	0.02	0.01	0.11	0.1	0.04	0.02
TiO_2 %	0.22	0.34	0.14	0.46	0.13	0.07	0.29	0.39	0.26
P_2O_5 %	0.05	0.08	0.03	0.05	0.04	0.03	0.1	0.13	0.1
Cr_2O_3 %	0.01	<0.01	0.01	0.03	0.02	0.04	0.03	0.04	<0.01
LOI %	1.75	1.85	1.8	2.6	1.4	2.85	1.8	0.5	2.5
SUM %	98.66	98.14	98.45	99.78	99.1	100.3	99.9	100.4	99.52
As ppm	<3	<3	<3	<3	<3	<3	<3	<3	30
Au ppb	210	90	30	40	20	<10	<10	<10	30
Sr ppm	40	50	10	30	20	170	290	980	<10
Y ppm	10	10	30	40	10	<10	<10	<10	110
Zr ppm	250	410	120	430	90	70	110	160	110

Appendix II : Table 2. Fluid Inclusions Data from San Lusi Deposit

Sample	Host Mineral	Inclusion type	Freezing Temp. (^{o}c)	Salinity Eq.Wt%	Homogen. Temp (^{o}c)	Location ore/nonore
KA1E	Quartz	P	-0.2	0.35	277	nonore
KA1E	Quartz	P	-0.2	0.35	277	nonore
KA1E	Quartz	P	-0.3	0.53	276	nonore
KA1E	Quartz	P	-0.4	0.71	277	nonore
KA1E	Quartz	P	-0.1	0.18	255	nonore
KA1E	Quartz	P	-0.3	0.53	260	nonore
KA1E	Quartz	P	-0.4	0.71	234	nonore
KA1E	Quatrz	P	-0.5	0.88	212	nonore
KA1E	Quartz	P	-0.3	0.53	265	nonore
KA1E	Quartz	P	0	0	218	nonore
KA1E	Quartz	P	0	0	218	nonore
KA1E	Quatrz	P	0	0	218	nonore
KA1E	Quartz	P	-0.2	0.35	244	nonore
KA1E	Quartz	P	-0.3	0.53	215	nonore
KA1E'	Quartz	P	0	0	277	nonore
KA1E'	Quartz	P	0	0	277	nonore
KA1E'	Quartz	P	0	0	277	nonore
KA1E'	Quartz	P	-0.1	0.18	276	nonore
KA1E'	Quartz	P	-0.1	0.18	277	nonore
KA1E'	Quartz	P	-0.3	0.53	278	nonore
KA1E'	Quartz	P	-0.2	0.35	277	nonore
KA4	Quartz	P	-0.7	1.23	270	ore
KA4	Quartz	P	-0.6	1.05	275	ore
KA4	Quartz	P	-0.2	0.35	245	ore
KA4	Quartz	P	0	0	255	ore
KA4	Quartz	P	-0.1	0.18	265	ore
KA4	Quartz	P	-0.6	1.05	245	ore
KA4	Quartz	P	-0.9	1.57	250	ore
KA4	Quartz	P	-1	1.74	250	ore
KA4	Quartz	P	-0.9	1.57	210	ore
KA4	Quartz	P	-0.2	0.35	200	ore
KA4	Quartz	P	-1.2	2.07	230	ore
KA4	Quartz	P	-1.2	2.07	230	ore
KA5	Quartz	P	-7.8	12.62	145	nonore
KA5	Quartz	P	-8.4	12.16	171	nonore
KA5	Quartz	P	-8.4	12.16	171	nonore
KA5	Quartz	P	-8.2	11.93	175	nonore
KA5	Quartz	P	-8.2	11.93	171	nonore
KA5	Quartz	P	-8.3	12.05	170	nonore
KA5	Quartz	P	-8.1	11.81	171	nonore
Ka23B	Quartz	P	-0.2	0.35	276	nonore
KA23B	Quartz	P	-0.2	.035	276	nonore
KA23B	Quartz	P	-0.2	0.35	276	nonore

Appendix II : Table 2... continued

Sample	Host Mineral	Inclusion Type	Freezing Temp. (°c)	Salinity Eq. Wt %	Homogen. Temp.(°c)	Location ore/nonore
KA23B	Quartz	P	0	0	275	nonore
KA23B	Quartz	P	0	0	275	nonore
KA23B	Quartz	P	0	0	274	nonore
KA23B	Quartz	P	0	0	274	nonore
KA23B'	Quartz	P	-7.3	10.86	171	nonore
KA23B'	Quartz	P	-6.6	9.98	171	nonore
KA23B'	Quartz	P	-6.4	9.73	170	nonore
KA23B'	Quartz	P	-6.6	9.98	171	nonore
KA23B'	Quartz	P	-6.6	9.98	171	nonore
KA23B'	Quartz	P	-7	10.49	170	nonore
KA23B'	Quartz	P	-7.6	11.34	172	nonore
KA26	Quartz	P	-3.1	5.11	205	ore
KA26	Quartz	P	-2.9	4.80	207	ore
KA26	Quartz	P	-3.4	5.56	203	ore
KA26	Quartz	P	-3.3	5.41	202	ore
KA26	Quartz	P	-3.6	5.86	200	ore
KA26	Quatrz	P	-4.1	6.16	197	ore
KA26	Quartz	P	-4.1	6.16	198	ore
KA26	Quartz	P	-3	4.96	197	ore
KA26	Quatrz	P	-3.1	5.11	198	ore
KA26	Quartz	P	-3.2	5.26	200	ore
KA26	Quartz	P	-3.5	5.71	196	ore
KA26	Quartz	P	-3.6	5.86	206	ore
KA26	Quartz	P	-4	6.45	205	ore
KA26	Quartz	P	-3.9	6.30	208	ore
KA27	Quartz	P	-8.8	11.46	163	nonore
KA27	Quartz	P	-8.8	11.46	163	nonore
KA27	Quartz	P	-8.3	12.05	177	nonore
KA27	Quartz	P	-7.6	11.22	172	nonore
KA27	Quartz	P	-8.3	12.05	172	nonore
KA27	Quartz	P	-4.9	7.73	183	nonore
KA27	Quartz	P	-4.9	7.73	183	nonore
KA28	Quartz	P	-0.3	0.53	270	nonore
KA28	Quartz	P	-0.8	1.4	270	nonore
KA28	Quartz	P	-0.8	1.4	270	nonore
KA28	Quartz	P	-0.8	1.4	270	nonore
KA28	Quartz	P	-4.8	7.59	276	nonore
KA28	Quartz	P	-4	6.45	278	nonore
KA28	Quartz	P	-4	6.45	277	nonore
KA29	Quartz	P	-0.3	0.53	222	nonore
KA29	Quartz	P	-0.3	0.53	222	nonore
KA29	Quartz	P	-0.9	1.57	212	nonore
KA29	Quartz	P	-0.8	1.4	212	nonore

Appendix II : Table 2....continued

Sample	Host Mineral	Inclusion Type	Freezing Temp.(°c)	Salinity Eq. Wt %	Homogen. Temp.(°c)	Location ore/nonore
KA29	Quartz	P	-1	1.74	211	nonore
KA29	Quartz	P	-0.1	0.18	224	nonore
KA29	Quartz	P	-2	3.39	210	nonore
KA29	Quartz	P	-1.3	2.24	215	nonore
KA29	Quartz	P	-1.2	2.07	212	nonore
KA29	Quartz	P	-1.8	3.06	210	nonore
KA29	Quartz	P	-1.1	1.91	214	nonore
KA29	Quartz	P	-1	1.74	211	nonore
KA29	Quartz	P	-2.9	3.23	210	nonore
KA29	Quartz	P	-1.5	2.57	210	nonore
KA1E'	Quartz	S	0	0	158	nonore
KA1E'	Quartz	S	-0.3	0.53	169	nonore
KA1E'	Quartz	S	-0.2	0.35	169	nonore
KA1E'	Quartz	S	-0.2	0.35	169	nonore
KA1E'	Quartz	S	-0.3	0.53	156	nonore
KA1E'	Quartz	S	-0.3	0.53	156	nonore
KA1E'	Quartz	P	0	0	279	nonore
KA5	Quatrz	S	-0.3	0.53	170	nonore
KA5	Quartz	S	-0.4	0.71	171	nonore
KA5	Quartz	S	-0.2	0.35	170	nonore
KA5	Quartz	S	-0.3	0.53	170	nonore
KA5	Quartz	S	-0.4	0.71	173	nonore
KA5	Quartz	S	-0.1	0.18	172	nonore
KA5	Quartz	S	-0.2	0.35	175	nonore
KA23B	Quartz	S	-0.3	0.53	185	nonore
KA23B	Quartz	S	-0.3	0.53	185	nonore
KA23B	Quartz	S	0	0	182	nonore
KA23B	Quartz	S	0	0	150	nonore
KA23B	Quartz	S	0	0	185	nonore
KA23B	Quartz	S	0	0	185	nonore

ore : > 890 ppb Au
nonore : < 890 ppb Au

Appendix III : Table 3. Gas Analyses Data

Sample	KA29	KA1E	KA1E'	KA23B	KA23B'	KA26	KA27	KA4	KA28
H_2 %	2.6973	4.7399	1.5743	0.000	9.4131	0.6485	0.9605	0.7984	3.6959
He mol %	0.000	0.000	0.000	0.000	0.000	0.000	0.000	0.000	0.000
Ar mol %	0.0009	0.000	0.000	0.0005	0.0005	0.0005	0.0115	0.0004	0.0071
N_2 mol %	0.0842	0.0335	0.0265	0.0189	0.1058	0.0508	1.6069	0.1635	1.0243
Co mol %	0.7094	0.2832	0.2492	0.0167	3.8366	0.3600	0.2162	0.4631	0.3894
CH_4 mol %	0.2001	0.3688	0.2117	0.0004	2.1461	0.0881	0.2644	0.1744	0.2383
CO_2 mol %	1.0327	16.3729	10.2547	25.3399	13.8760	6.8994	9.7746	6.2145	18.4275
H_2S mol %	0.0078	0.0123	0.2499	0.2246	0.1088	11.9415	5.6399	2.5225	4.5982
C_nH_n mol%	0.49637	0.5134	0.674	5.1746	4.43646	0.83037	0.37804	0.52025	1.26813
H_2O %	94.72	77.67	86.76	71.20	64.07	77.97	81.06	89.09	70.11
Location	nonore	nonore	nonore	nonore	nonore	ore	nonore	ore	nonore

ore : > 890 ppb Au
nonore : < 890 ppb Au

Appendix IV : Sample Location and Numbers

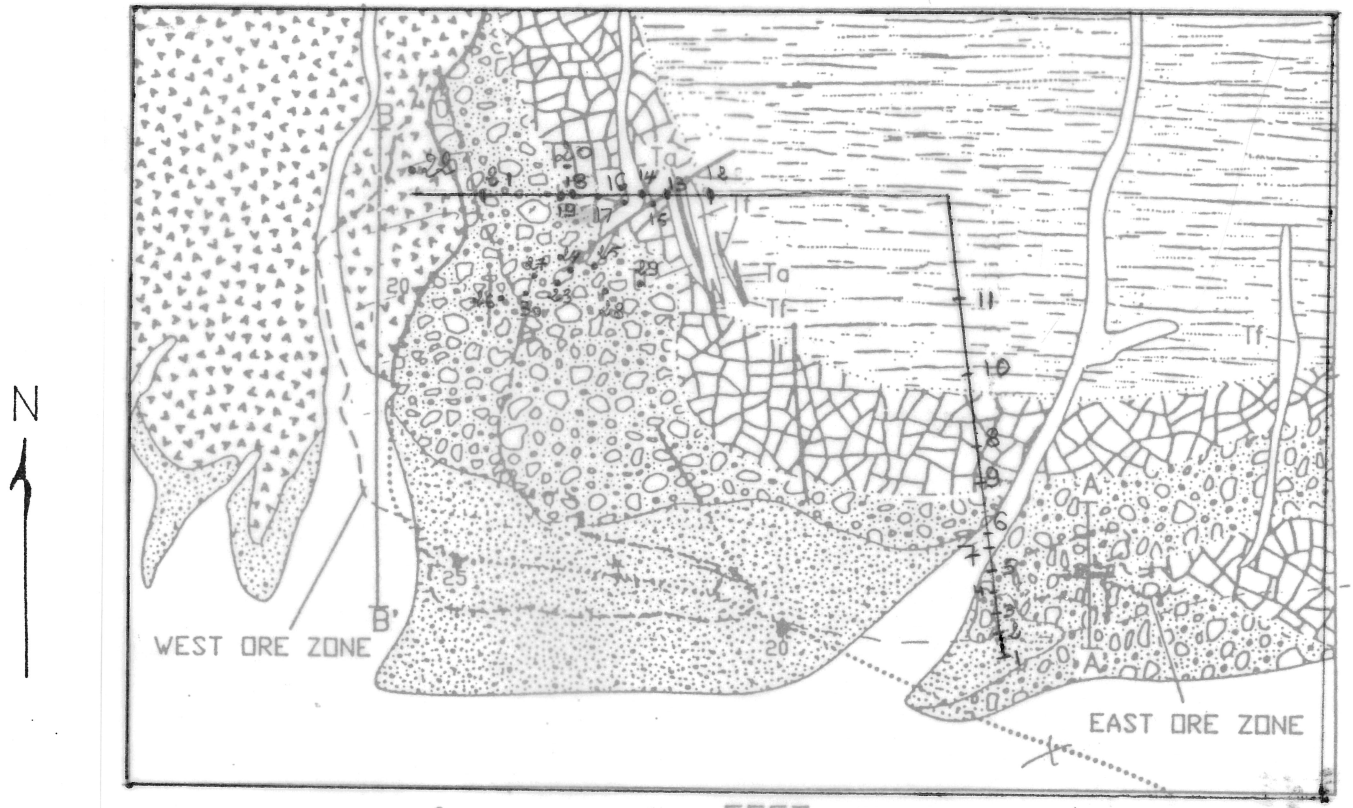
N
WEST ORE ZONE
EAST ORE ZONE
B
B'
A
A'
Ta
Tf
0 1000 FEET 2000 3000
0 1 2 3 4
KILOMETERS
LOCATION OF MAP AREA
map area
San Luis
0 mi.s 7
0 km.s 7
Tertiary
Precambrian
alluvium
Santa Fe Formation
andesite
felsite
biotite gneiss breccia
biotite gneiss cataclasite
gneissic granite
biotite gneiss
faults (dotted where inferred)
surface projection of ore contours (>0.0169 oz/st Au
detachment fault, teeth on hanging wall (dotted where inferred)